Chapter 4

Morphology and Phase Transitions of the d-Al-Ni-Co Surfaces

The equilibrium morphology of crystal surfaces is determined by the surface free energy, which contains surface and step energies. In periodic crystals there is only a limited number of different parallel net planes, leading to a finite number of energetically different surface terminations. In contrast, a quasicrystalline ordering perpendicular to the surface supports infinitely many structurally inequivalent terminations. Moreover, the step heights separating similar planes can be incommensurate, as opposed to steps between equivalent planes in periodic crystals. Under these conditions it is not trivial to estimate the surface and step energies in quasicrystals and to determine the energetically favored morphology. Hence, it is important to characterize the morphology of quasicrystalline surfaces.

The fivefold surface of icosahedral Al-Pd-Mn [65-74] and the tenfold surface of decagonal Al-Ni-Co [11, 13, 22, 75] have been intensively studied at room temperature, and few reports on the twofold surfaces of d-Al-Ni-Co have been published [11, 76]. In contrast, quasicrystalline surfaces have not yet been investigated at all at high temperature.

Consequently, no knowledge exists regarding the surfaces' structural or morphological properties of the high-temperature bulk Al-Ni-Co phases. While these constitute an interesting topic themselves, undergoing any surface phase transition during sample preparation (usually cycles of sputtering and annealing) for room temperature experiments might influence the properties, if the equilibrium is not reached. Indeed, the surface morphology at room temperature has been found to differ significantly depending on the sample's heating history, e.g. a clustered as well as a terraced morphology has been observed by RT-STM for previous annealing at medium and high temperatures, respectively [13]. Low-temperature STM investigations show two different terminations within the same surface [77, 78].

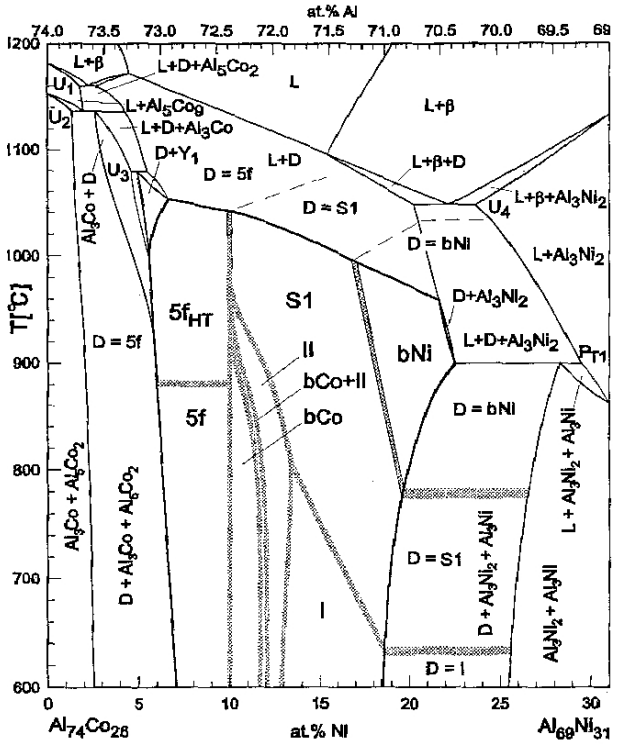

Figure 4.1: Section of the Al-Ni-Co phase diagram along the composition line $Al_{74}Co_{26}$ -$Al_{69}Ni_{31}$ from Ritsch et al. [8] with I, S1, and bNi denoting type I, S1, and basic Ni decagonal modifications, respectively.

The bulk phase diagram of Al-Ni-Co has been mapped in great detail [79-81] and a variety of decagonal modifications has been identified [8, 82]. However, the mechanisms of the bulk phase transitions are yet unknown.

In this chapter, investigations by low-energy electron microscopy (LEEM) (recorded at the University of Essen in the group of Prof. Horn-von Hoegen) of the tenfold (00001)-, and the two inequivalent (10000)- and (001$\bar{1}$0)- twofold surfaces of d-$Al_{72.3}Ni_{18.2}Co_{9.5}$ are presented. The observation temperature ranges from 20 - 850 ° C. Two surface phase transitions are identified by a change in morphology. Their transition temperatures are close to those expected for structural bulk phase transitions. Possible mechanisms which could explain the observed changes in surface morphology as the phase transitions are occurring are discussed.

4.1 Decagonal Modifications in the Phase Diagram of Al-Ni-Co

The first stable decagonal phase was reported by Tsai et al. in the compositional range of $Al_{70}Ni_{15}Co_{15}$ in 1989 [83], leading to a reinvestigation of the Al-Ni-Co phase diagram [84-88]. The existence region of the decagonal phase has been found to be an area of almost constant Al-concentration (around 72%) with varying Ni and Co content.

After the discovery of a new type of quasicrystal within the decagonal phase by Edagawa et al. [89], Ritsch et al. have systematically studied the stability region of decagonal Al-Ni-Co and have identified eight distinct structural modifications [8]. The classification of the samples has been done by transmission electron microscopy. The samples were obtained by quenching the homogenized melt of appropriate composition from the corresponding temperature. The existence regions of different modifications are separated by thick dotted lines in figure 4.1. Samples quenched from a composition on these thick lines, show characteristics of both adjacent modifications, although at least one of the sets of characteristic Bragg reflections is diffuse or only very weak. However, this observation does not necessarily signify a real transition state, since the investigated sample area was up to 1 μm in diameter. Thus, it was not possible to distinguish between a local transformation and domain formation, i.e, between a second and first order transformation. Only for the transition between the modifications S1 and basic Ni do the authors conclude a local transition based on high-resolution transmission electron micrographs [8]. Dilatometric investigations agree with this subdivision of the phase diagram [81] and indicate second order transformations between all modifications.

Generally, the modifications can be distinguished by [8]:

(i) composition and temperature,
(ii) superstructure reflections in the quasicrystalline layers,
(iii) existence and modulation of layers of diffuse scattering,
(iv) tilings (shape of tiles and random vs. ideal ordering of these),
(v) symmetry and ordering of the atom clusters,
(vi) ordering state (chemical or topological order), and
(vii) periodicity along the tenfold rotational axis.

The sample investigated by LEEM is of composition $Al_{72.3}Ni_{18.2}Co_{9.5}$ and therefore cannot be found in the phase diagram depicted in figure 4.1. However, a useful estimation of its temperature dependence can be gained by the represented cut of the phase diagram as this is sufficiently close to our sample composition to allow an extrapolation of the results from the diagram to the sample. Hence, for this composition, three different decagonal phases (type I, S1, and basic Ni) can be expected in the temperature range from 20 - 850 °C.

Before analyzing the data from those three modifications, their structural characteristics are

Phase	Superstructure Reflections	Layers of Diffuse Scattering	Tiling Type	Cluster Symmetry	Periodicity
Basic Ni	-	no	perfect pentagonal	10-fold	4 Å
S1	S1	yes	random pentagonal	5-fold	8 Å
Type I	S1 + S2	yes	random rhombic	5-fold	8 Å

Table 4.1: Overview of different quasicrystalline phases of Al-Ni-Co with their structural characteristics.

presented. A first overview is given in table 4.1, while a detailed description follows.

4.1.1 Diffraction Patterns of the type I, S1 and Basic Ni Modification

The first criteria for the distinction of the decagonal modifications in d-Al-Ni-Co are their diffraction patterns. The basic Ni modification can be considered as the basic decagonal phase [90] from which the other ones are derived. The diffraction pattern of the tenfold sample orientation consists of sharp Bragg reflections at fundamental reciprocal lattice points and almost no diffuse scattering intensity. The diffraction patterns of the twofold orientations show only the basic 4 Å periodicity.

The diffraction patterns of the S1 and type I modifications show additional diffraction spots in the quasicrystalline planes, diffuse scattering intensity in planes perpendicular to the tenfold axis and a doubling of the periodicity to 8 Å along the tenfold axis. The additional reflections in the quasicrystalline plane can be regarded as superstructure spots, if the concept of superstructure ordering in conventional crystals is adapted to quasicrystals. The basis for this generalization lies in the description of a quasicrystalline structure as a section of a higher dimensional periodic structure. The superstructure ordering in a quasicrystal is then defined as a superlattice order in the corresponding periodic lattice of higher dimension [82].

While the diffraction pattern of the basic Ni phase shows only fundamental reflections characterized by multiples of the basis vectors, the type I and S1 structure exhibit additional diffraction spots, which Edagawa has indexed by 1/5 x integers [89]. Thus, the five-dimensional periodic structure has a superstructure with the same point group symmetry as the fundamental lattice but a five times enlarged unit cell. The reflections are classified as S1 and S2 reflections [82]. The type I modification shows both S1 and S2 reflections.

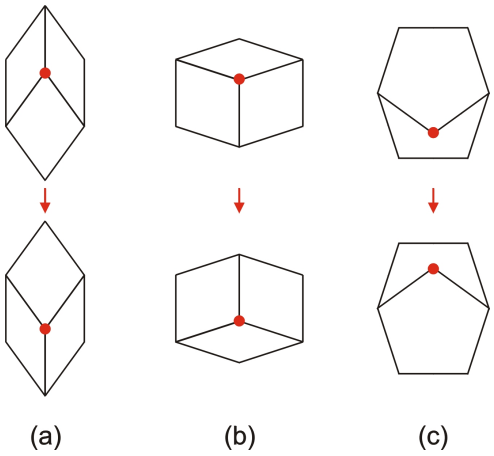

Figure 4.2: Illustration of phason flips inside hexagons in the rhombic (a,b) and pentagonal tiling (c). The red dot indicates the jumping vertex.

4.1.2 Tiling Types and Ordering

The structural description of quasicrystals in higher dimensional space, as introduced in chapter 2, shows atomic positions in real space to be derived from a section of a higher dimensional periodic lattice. A more intuitive way to describe the nature of quasicrystalline structures is the tiling-cluster model. The tiling describes an aperiodic lattice, whose vertices are decorated by atomic clusters. For the class of decagonal quasicrystals, the two-dimensional quasicrystalline plane is covered by a rhombic or pentagonal tiling and columnar clusters are located at its vertices.

The tilings can be divided into two classes: ideal and random tilings. An ideal tiling can be constructed by projection from higher dimensional space as was shown for the 2-dimensional Penrose tiling in chapter 2. The random tiling can be obtained from the ideal quasiperiodic tiling by the introduction of phason flips. These are defined as local rearrangements of points, in this case the vertices of the tiling. An illustration of possible phason flips in rhombic and pentagonal tilings is shown in figure 4.2. In the rhombic tiling single flips can be described as a vertex jump inside hexagons composed of either two skinny and one fat rhombi or two fat and one skinny rhombi. In the pentagonal tiling a phason flip is likewise a vertex jump in a hexagon.

A systematical analysis of the decagonal Al-Ni-Co modifications has shown that only the basic Ni type exhibits an ideal quasiperiodic tiling while all other modifications have random tilings [91]. The basic Ni structure is a high-temperature phase encountered above 750°C [8]. As the temperature is lowered the alloy transforms into a different decagonal phase with a random tiling.

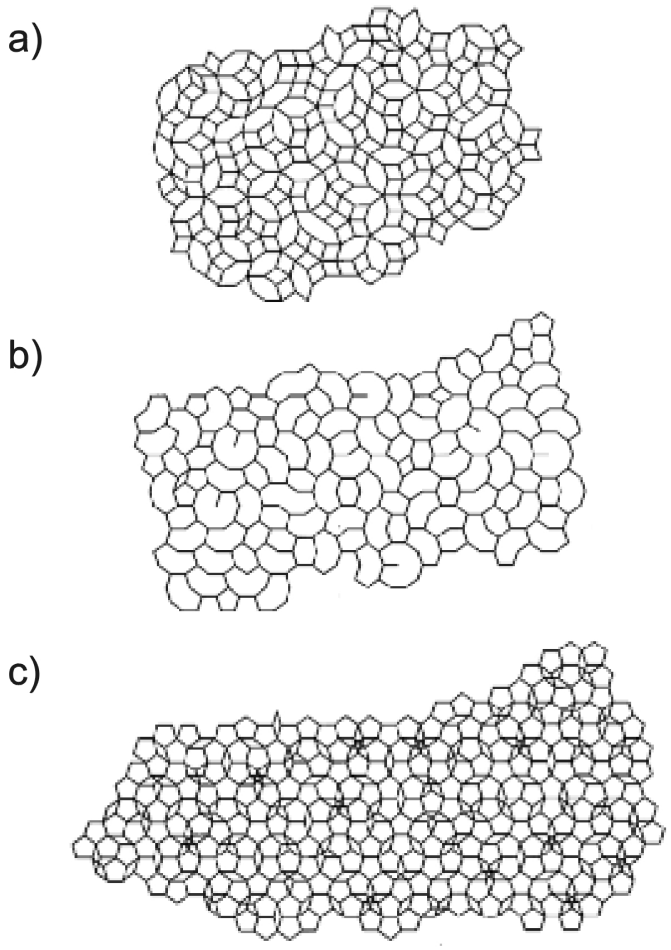

Figure 4.3: Characteristic quasicrystalline tilings for (a) type I phase, (b) S1 phase, and (c) basic Ni phase, observed by transmission electron microscopy by Joseph et al. [91].

From the point of view of the stabilization mechanism this contradicts all expectations of an energetically stabilized ideal tiling and an entropically stabilized random tiling, which by phasonic entropy should be favored at high temperature. In order to resolve this contradiction Joseph et al. suggested that chemical entropy plays an important role in the stabilization mechanism [91]. Their calculations showed that a disorder between the transition metal atoms would be sufficient to compensate the entropy loss due to an ideal tiling. Indeed, experimental evidence of a chemical disorder not just between Ni and Co, but between Al and the transition metal atoms was found some time later by Yan et al. [92]. In addition, one indication for chemical ordering in the low-temperature type I phase is the increase of periodicity along the tenfold axis as will be discussed in section 4.1.4.

The transformation between the tilings involves a multitude of single atom phason flips,

which eventually result in a phason flip of a whole cluster and finally in a change of tiling type. In contrast to diffusion, where atoms leave their original position to occupy a vacant lattice site, atomic phason flips are a change in the lattice itself. The atoms jump into new lattices sites, whereby the original positions are no longer lattice sites anymore. Usually these jumps occur over lengths smaller than the nearest neighbor distances. Therefore, prerequisites for atomic phason flips are half-vacancies in order to preserve the minimum atomic distances before and after the jump.

Although deflation or inflation of the above described tilings yields an equivalent tiling with τ-scaled edge length, the edge length usually referred to is 19.78 Å. This is due to the fact that the experimentally most easily observable structural features are the 19.78 Å-clusters located at the tilings' vertices.

4.1.3 Atomic Clusters in the Decagonal Modifications

Depending on the kind of quasicrystalline superstructure, not only the arrangement of clusters changes (i.e., the tiling) but also the atomic distribution within the clusters. In all modifications, the clusters are columnar clusters with 19.78 Å diameter and aligned parallel to the periodic axis. Each of their atomic planes has fivefold symmetry, and its orientation alternates by 180° in adjacent planes.

While in almost all modifications the columnar cluster itself has a fivefold symmetry, the fundamental basic Ni phase is the only phase with tenfold symmetric clusters. This increased symmetry is due to a chemical disorder of the atoms within the clusters. The first direct evidence of chemical disorder between Al and the transition metal atoms was found in high-resolution electron transmission microscopy images [92].

In the cluster model, an explanation for the occurrence of superstructure diffraction spots can be found in different relative orientations of the fivefold symmetric clusters. While a random distribution only shows the fundamental spots, an inverse orientation of neighboring clusters on the rhombic tiling gives rise to the additional S1 and S2 Bragg reflections [93]. Decorating a pentagonal tiling by alternating cluster orientations results in the S1 superstructure.

4.1.4 Periodicity along the Tenfold [00001]-Axis

As mentioned previously, an increase in periodicity along the tenfold rotational axis is found in several of the modifications. A 4 Å periodicity is only encountered in the high-temperature basic Ni phase, while the S1 and type I modifications show a doubling of this periodicity.

The main periodicity of 4 Å is ascribed to a stacking of fivefold quasicrystalline planes with a distance of 2 Å, where the planar cluster cuts in consecutive planes are related by inversion

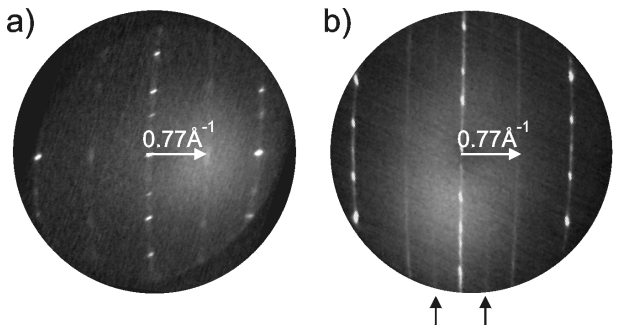

Figure 4.4: LEED patterns of (a) the (10000)-, and (b) the (001$\bar{1}$0)- surface of the type I phase of d-$Al_{72.3}Ni_{18.2}Co_{9.5}$ recorded in the LEEM instrument at about 200 °C and 100 °C, respectively. The arrows mark a weak 16 Å periodicity.

symmetry.

The origin of the 8 Å periodicity in the S1 and type I modifications is still under debate. Early models anticipated a chemical ordering of the atomic species [94], while the latest model by Cervellino et al. has a more complex solution [42]. It suggests a sequence of flat and puckered quasicrystalline atomic layers along the tenfold axis. The displacement of atoms of the puckered layers alternate in direction, thus producing a doubling of the basic periodicity. Their model of the 8 Å periodicity is thus an extension of the earliest idea of out-of-plane Al atoms being responsible for the doubling the periodicity [95]. In order to explain the occurrence of diffuse scattering in the planes of quasicrystalline Bragg reflections, Cervellino predicted the existence of columnar domains of infinite extension along the periodic axis, but finite extension in the quasicrystalline plane [42]. These domains are shifted parallel to the periodic axis by 4 Å in a random distribution.

Additionally, a 16 Å-periodicity can be observed in the low energy electron diffraction patterns at room temperature of the twofold surfaces of $Al_{72.3}Ni_{18.2}Co_{9.5}$ as indicated in figure 4.4. This is not incorporated in any structural model so far. The first observation of this increased periodicity was made only recently on the (10000)-surface of a sample with composition $Al_{71.8}Ni_{14.8}Co_{13.4}$ (this sample also belongs to the type I superstructure phase at room temperature) [77]. Since this increase in periodicity is observed on differently oriented samples and different composition, a pure surface reconstruction can be ruled out and this feature can be considered as a structural characteristic of the type I phase. With only the LEED data at hand, it is difficult to propose a detailed model for this feature. However, an additional chemical ordering could produce such an effect.

4.2 LEEM Investigations of the d-Al-Ni-Co Surfaces

Some experimental considerations have to be taken into account before interpreting the acquired LEEM data. These are briefly described in this section.

All samples were polished by diamond paste from 6 μm down to 0.5 μm previous to insertion into the LEEM apparatus to rule out 'history' effects. Preceding the first LEEM measurements, the samples were sputtered by Ne^+ (3 keV). Unfortunately, the first annealing of the samples could not be monitored due to excessive degassing. Usually, the samples were annealed by increasing the temperature in several steps up to 850 °C, such that the pressure in the UHV chamber did not exceed 5×10^{-8} mbar.

The temperature of the sample was measured by an infrared pyrometer, with the emissivity of the quasicrystal approximated by that of Al. Since there was no other possibility to check the temperature, the error is estimated to ±50 °C. Any temperatures given in the following are thus to be understood with this systematic uncertainty.

The first investigations were used to gain an overview of the morphological features of the different samples upon annealing. Therefore, the samples were heated from room temperature to the highest temperature of 850 °C in an interval of about 2 hours and similarly cooled down. Subsequent experiments were focused on different aspects, such as the influence of rapid or slow temperature changes and phase transitions, and carried out accordingly.

To derive reliable information about morphological characteristics at a certain temperature, it is necessary to assure the surface is well equilibrated. In general, this can be achieved by keeping the sample at the investigation temperature for an extremely long time. Since this is not practicable it is instructive to get an estimate of the required time interval to get an equilibrated surface. One approach is to monitor step motion through a single point defect. If the step impinges on such a barrier, it will be pinned and thus lose its equilibrium shape resulting in a convex deformation. The elongation of the step implies an increase in total step energy, which yields a surface diffusion flux finally regaining the equilibrium step shape. Above 650 °C, the necessary time to obtain the equilibrium amounts to a few seconds, decreasing with even higher temperature. Below 650 °C the roughness of the sample (as will be shown in the following sections) does not allow this kind of measurement.

While the consideration of step shapes focused on surface diffusion, an equilibrium between bulk and surface is determined by bulk diffusion. For example, structural bulk transitions, as they will be encountered in d-Al-Ni-Co, are related to changes in the amount of bulk structural vacancies. The equilibration of the bulk proceeds via a material exchange with the surface. There, step edges can serve as sinks or sources for bulk vacancies by releasing atoms to or adsorbing atoms from the bulk, respectively [96]. Consequently, such a material exchange is

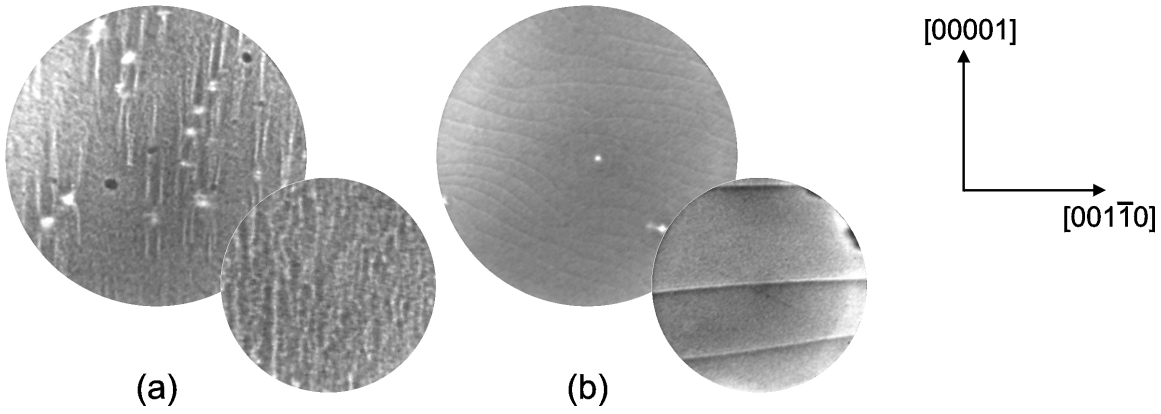

Figure 4.5: Morphological characteristics of the (10000)-surface at (a) about 300 °C, and (b) 780 °C. The large and small circle comprise a field of view of 83 μm and 6.7 μm, respectively. While the high temperature phase exhibits large terraces without any predominant step orientation, at low temperatures the much smaller terraces are elongated along the periodic [00001] direction.

detectable by step motion as well. In this case, the equilibrium is more difficult to determine and is also dependent on the surface diffusion.

One additional problem in investigating alloy phases is its possible decomposition at high temperature. In this case the preferential evaporation of Al might be feared. The highest temperature reached in the experiments was about 850 °C, a temperature up to which a constant stoichiometry has been observed [97].

4.3 Temperature Dependent Morphology of d-Al-Ni-Co

In this section investigations of the twofold (10000)-, the tenfold (00001)-, and the twofold (001$\bar{1}$0)-surfaces of d-Al-Ni-Co by mirror electron microscopy (MEM) are presented in order to gain an overview of their morphological characteristics. It is shown that these three surfaces exhibit a qualitatively similar morphology evolution with temperature.

4.3.1 Morphology of the Twofold (10000)-Surface

The surface of the twofold d-$Al_{72.3}Ni_{18.2}Co_{9.5}$(10000) shows two significantly different morphologies in the investigated temperature range. Below about 650 °C the surface is rough on the nm-scale (figure 4.5 (a)), while at higher temperatures the surface exhibits flat terraces of several μm size (figure 4.5 (b)). The transition between the rough and smooth surface is very abrupt, confined to a temperature of about 650 °C. In order to understand the image in figure 4.5 (a) the transition is followed in figure 4.6.

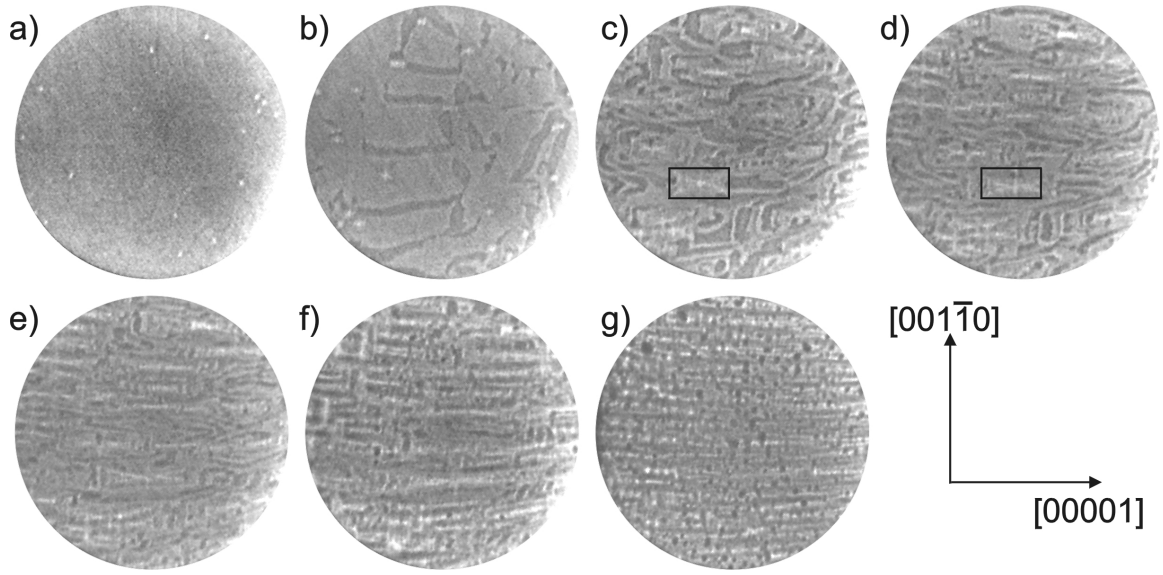

Figure 4.6: LEEM images of the (10000)-surface upon roughening at 650 °C. The sequence was recorded within a few minutes during cooling from 670 - 500 °C. The image in (a) was not defocused to observe the steps as it was in figure 4.5, but to monitor the following phase transition and thus the phase contrast as in (b). The circle in (c) points out one of the mass sources, which can be considered as a channel to the bulk. The material is then distributed by surface diffusion. The images have a diameter of 40 μm.

Starting from a smooth surface at 700 °C cooling induces a phase contrast to appear at step edges. The contrast then spreads over the adjacent terrace parallel to the step alignment. The LEED pattern does not change its appearance drastically, indicating both terminations to be of a common quasicrystalline order with only slightly different structure factor. On the basis of the MEM data it cannot be determined whether this termination is a reconstruction of the originally exposed plane or an additional layer created by atoms being removed from, or added to the surface from the bulk.

In order to investigate this beginning of the transition in more detail, larger magnification images are depicted in figure 4.7. Likewise, phase contrast can be observed, separated by steps from the original termination. While the step shape could not be resolved in the larger image sections of figure 4.6 (b), figure 4.7 (c-g) show that the steps lose their equilibrium shape (figure 4.7 (c-g)) and form 'fingers' aligned parallel to the periodic axis of the sample. This indicates an insufficient surface diffusion along the quasicrystalline direction.

The transition is now followed further in figure 4.6 (c-g). Material sources can be found at several places on the sample, one of these being marked by a rectangle in figure 4.6 (c,d). Here

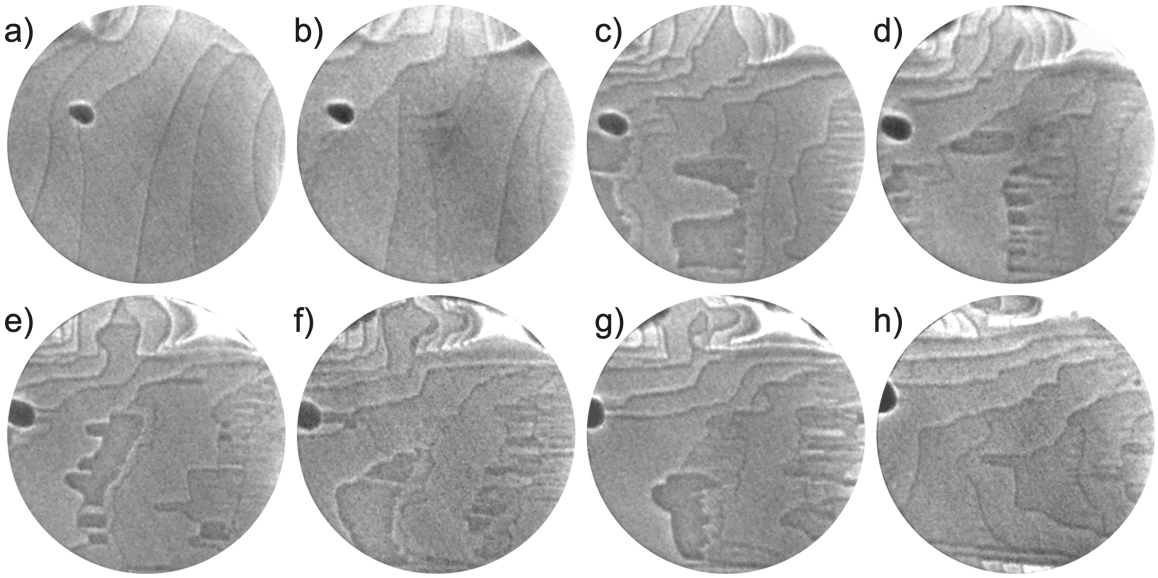

Figure 4.7: Larger magnification MEM images of the (10000)-surface at the beginning of the roughening (corresponding to figure 4.6(a-c)). Each image has a diameter of 4 μm. The image orientation is the same as an figure 4.6

much more material arrives at the surface than could be accumulated at existing step edges. These sources can thus be considered as channels into the bulk, which by bulk diffusion parallel to the surface are filled with material then being 'channeled' to the surface. By surface diffusion the released material is distributed over the surface area. Clearly, a dominant diffusion direction along the periodic axis can be observed, as already inferred from the step shape at the onset of the phase transition.

Considering the structural model of d-Al-Ni-Co, this preferential direction is not surprising. Along the periodic axis, atoms are aligned in the clusters, thus forming trenches for a continuous diffusion. The steps, naturally also all newly created steps, are simultaneously acting as sources or sinks for bulk vacancies.

Altogether this leads to an immense increase in the step density, which can no longer be resolved (figure 4.5 (a)). Hence, the at first sight seemingly disordered surface actually consists of a large number of steps and terraces. The corresponding LEED pattern, as depicted in figure 4.4 (a), reveals a quasicrystalline ordering with bulk derived diffraction spots.

The morphological roughening is reversible, i.e., the surface reverts to large terraces upon heating as illustrated in figure 4.8. The multitude of steps can again transfer mass to the bulk, resulting in their movement across the terraces. Eventually steps join to form larger terraces, while additional material from the bulk channels, one of them located just outside the lower left

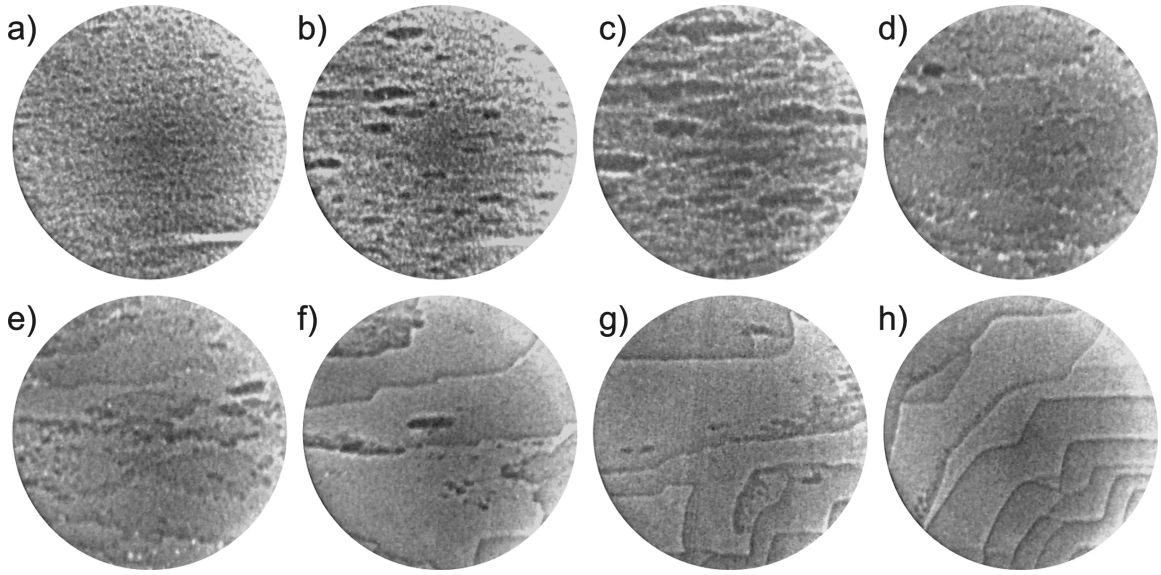

Figure 4.8: MEM images of the (10000)-surface by heating through the surface smoothing phase transition. Each image has a diameter of 8.3 μm. The [00001]-axis corresponds to the horizontal in these images.

part of the images, is also joining the steps. Finally, this process leads to μm-large terraces.

The large material exchange with the bulk indicates a strong influence of the latter on the events on the surface. Indeed, a bulk structural phase transition, namely between the modifications type I and S1, is expected around the temperature of the observed reversible surface transformation. To further support the close relationship between bulk and surface and to check whether a similar material exchange can be found two other sample orientations were investigated in this temperature range.

4.3.2 Morphology of the Tenfold (00001)-Surface

The tenfold (00001)-surface has been investigated under similar conditions as the twofold-surface in the preceding section. At room temperature and up to 650 °C this surface orientation also exhibits a very rough morphology on the nm-scale as represented in figure 4.9 (a). Here, the most outstanding features are black circles of different diameter, between which roughness can be observed. Since the images are recorded in a defocus condition which increases contrast and enlarges all features the size of the features is falsified. The sizes strongly depend on the defocusing condition indicating very steep slopes. As steep hills would not survive very long at temperatures up to 650 °C, the corresponding features are channels into the bulk as they have been observed on the twofold (10000)-surface in the previous section. Similarly to those findings,

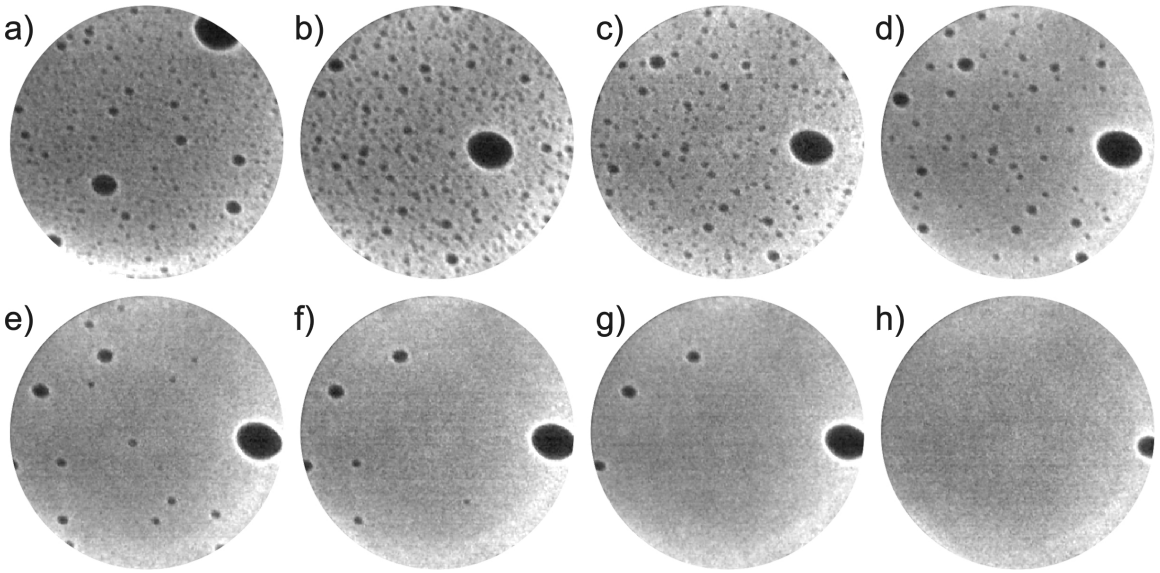

Figure 4.9: MEM images of the tenfold (00001)-Al-Ni-Co surface at (a) 300 °C. Due to thermal drift (b-h) are shifted downwards from (a) by about 20 μm. The temperature range is 650-700 °C. All circles comprise a field of view of 55.4 μm

a phase transition occurs around 650 °C, where the channels eventually vanish and terraces of several μm size develop. As long as there is even a marginal drift in temperature, the steps move very quickly across the surface, which makes them difficult to image.

This smoothing of the surface is reversible, since when the temperature is lowered holes appear again and an overall roughening can be observed. The transition temperature can be found around 650 °C in agreement with the transition on the twofold (10000)-sample. Unfortunately, the step motion cannot be imaged as clearly as on the twofold surface. Thus, a detailed description of the transition mechanism is not possible. However, by interpreting the holes as bulk channels in analogy to those found on the twofold surface an immense material exchange with the bulk can be inferred. Again, this indicates a close relationship with the bulk structural transition type I $\leftrightarrow$ S1.

Since the origin of the morphology at low temperature is not as easily tracked as on the twofold sample, its appearance is more difficult to imagine, and a brief comparison to STM images recorded on a sample of slightly different stoichiometry, namely $Al_{71.8}Ni_{14.8}Co_{13.4}$ is drawn in the following. Steep holes of about 30 nm diameter can be found, which can be related to the black circles found by MEM, therefore supporting the assumption of a channel formation for mass transport perpendicular to the surface. Between these channels, the STM investigations reveal a hill-and-valley morphology, created by a multitude of rough, 2Å high steps separating

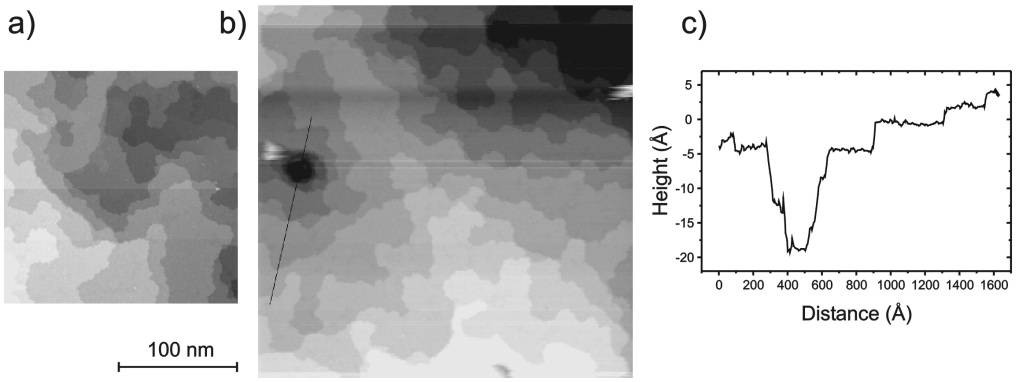

Figure 4.10: STM images (tunneling conditions: V = 2.02 V, I = 0.83 nA and V = 0.71 V, I = 0.48 nA for (a) and (b), respectively) (recorded in cooperation with H.R. Sharma, S. Fölsch and W. Theis) of the tenfold surface of $Al_{71.8}Ni_{14.8}Co_{13.4}$ at 7K. The sample had been prepared by sputtering and annealing to 700 °C. A multitude of images reveals an up- and down-morphology with terraces of about 100 Å width. The terraces are flat.

flat terraces of about 100 Å average width.

The step heights correspond to the distance of the quasicrystalline planes. Since no tendency of step pairing was observed, this indicates that these planes are energetically equivalent. The bulk structural model introduced in section 4.1.4 incorporates four different quasicrystalline layers, every second of them being buckled. Assuming that the random domains of displacements along the periodic axis do not determine the step locations, relaxation of the buckled layers towards equivalent flat layers at the surface can be inferred.

An analysis of high resolution STM images shows all planes to be structurally equivalent aside from the expected inversion symmetry of the fivefold clusters in adjacent planes [77, 98]. Other experimental investigations agree with this interpretation at room temperature [11, 13, 22, 75].

Since structural phase transitions in d-Al-Ni-Co are always associated to a structural change within the atomic planes only, the same interlayer distance is expected at temperatures above 650 °C. The mobility of the steps at high temperature can therefore be attributed to their low heights corresponding to single layer distances.

4.3.3 Morphology of the Twofold $(00\bar{1}\bar{1}0)$-Surface

The twofold $(00\bar{1}\bar{1}0)$-surface is flat at temperatures above 660 °C (as represented by the uppermost image in figure 4.11). In contrast to the tenfold orientation, steps can be observed. They do not move rapidly, indicating the formation of higher steps and/or higher step diffusion barriers.

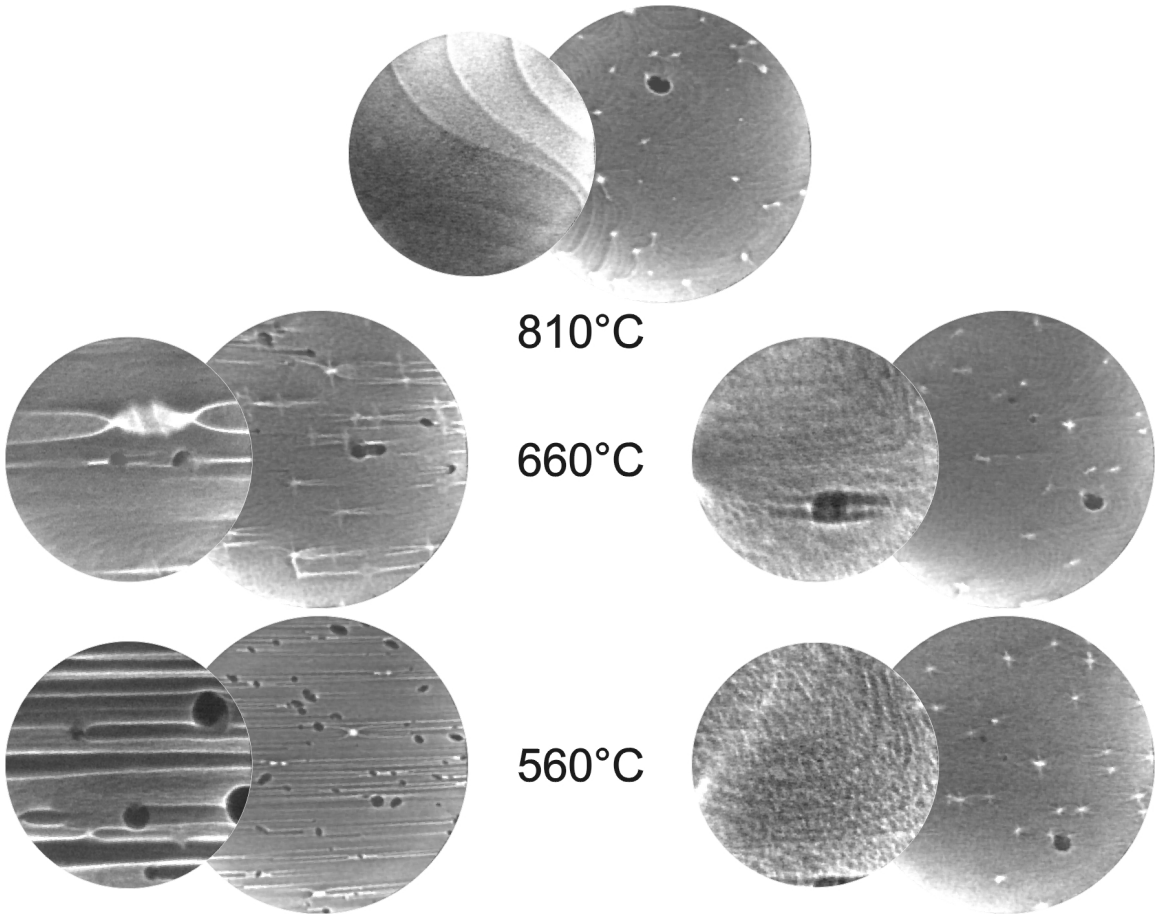

Figure 4.11: MEM images of the twofold $(001\bar{1}0)$-surface at 810 °C and during cooling. The left panel shows the surface during slow cooling, while the pictures on the right hand side were taken after the heating power was rapidly turned down. The morphology is found to be significantly different. The diameter of the large and small circles is 55.4 μm and 6.7 μm, respectively. The periodic axis is aligned with the images' horizontal. Not all images show the identical surface region, but they represent the morphology characteristic for the specified conditions.

Cooling the sample yields two significantly different morphological features. A rapid decrease in temperature leads to a sudden roughening of the steps at 660 °C and an overall rough surface on the nm-scale upon further cooling. However, this is clearly not an equilibrated surface, since if the temperature is slowly decreased (figure 4.13) or if the rough sample is held sufficiently long below 660 °C (figure 4.12), the resulting MEM images show pronounced stripes and darker imaged rims, all running along the periodic direction. Heating the sample back to temperatures above 660 °C results again in the flat step-terrace morphology. Hence, equivalently to the observations on the tenfold (00001)- and the twofold (10000)-surface, a reversible surface

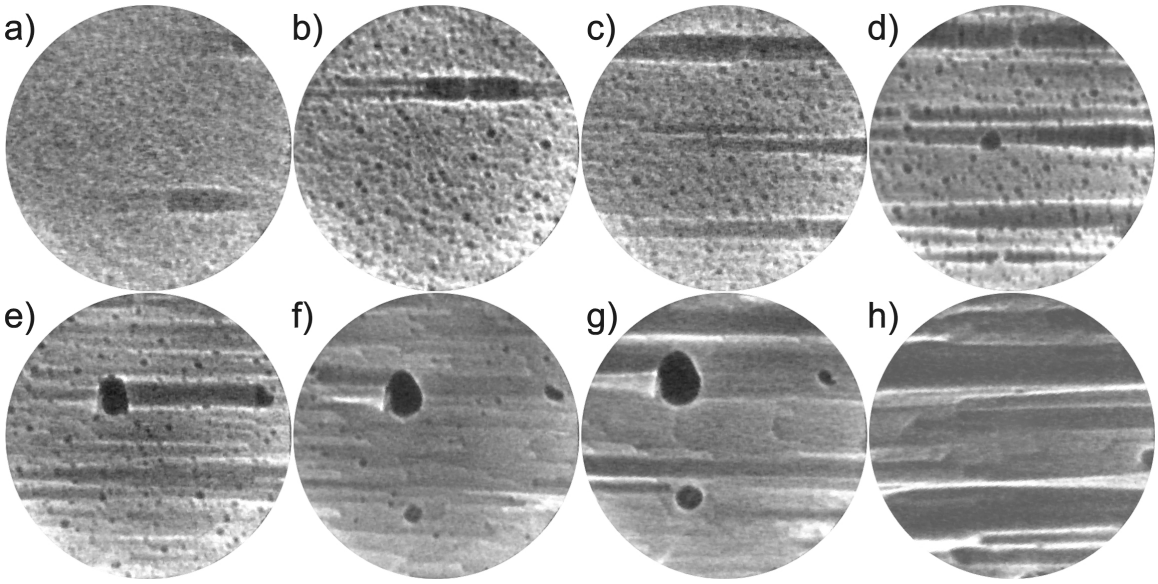

Figure 4.12: MEM images (6.7μm diameter, periodic axis of the sample parallel to horizontal) of the facet formation upon heating the rapidly cooled non-faceted (001$\bar{1}$0)-surface at (a) 558 °C, (b) after 1 min at 592 °C, (c) after 2 min at 600 °C, (d) after 3 min at 600 °C, (e) after 5 min at 624 °C, (f) after 8 min at 630 °C, (g) after 9 min at 630 °C, and (h) after 45 min at 630 °C. While (a)-(g) are recorded at the same location (except for some thermal drift), (h) is shifted by several μm.

phase transition is found at a temperature close to the bulk structural phase transformation type I $\leftrightarrow$ S1.

Before relating the morphological changes to any structural features it is necessary to understand the implications of these images. Therefore, it is useful to follow the evolution leading to this structure and its dissipation as will be done in the following.

4.3.4 The Faceting Process on the Twofold (001$\bar{1}$0)-Surface

Facet Formation

As already mentioned, rapidly lowering this surface's temperature results in a rough surface on the nm-scale. This is due to a large amount of step motion induced upon passing the transition temperature of about 660 °C. Three processes determine the kinetics: (i) surface diffusion to reach the equilibrium morphology, (ii) surface diffusion to the steep holes, serving as channels to the bulk and (iii) step edges acting as material (atom or vacancy) sources for the bulk. These processes had already been found on the other two sample orientations. Just as on the twofold (10000)-surface, the diffusion in this case is mainly directed parallel to the periodic direction, which had been explained by the straight atomic arrangements along this axis. Along the

quasicrystalline direction surface diffusion is very limited, such that smooth step edges cannot be maintained over large distances anymore. This results in a rough morphology.

However, this is not the equilibrium morphology of the presently investigated $(001\bar{1}0)$-surface at temperatures below 660 °C. If the sample is kept at temperatures below the transition but sufficiently high to allow diffusion, the morphology changes significantly as described in the following.

Since the sample was quenched from high temperatures, almost no bulk channels had evolved. Heating now induces these channels to be formed as can be seen in figure 4.12 (b-c). These 'ripen' to few steep channels (figure 4.12 (d-g)). The material exchange with the bulk predominantly proceeds via these channels, which therefore impose large gradients on surface diffusion. They are now responsible for a substantial mass transfer over long distances (up to several μm) on the surface. Again the direction is mainly along the periodic axis, readily explained by reduced surface diffusion perpendicular to the atomic rows. In addition to the diffusion gradient to the bulk channels, surface diffusion occurs in order to reach the equilibrium morphology. However, its influence is obscured by the immense gradient to the bulk channels.

Since the mass flux on the surface is restricted to the periodic sample direction and predominantly driven by the gradient to the bulk channels, these rims will eventually adjoin an area with no flux, less flux or oppositely directed flux. At these borders steps will accumulate, which are all aligned with the periodic axis of the sample. While it is in principle possible that this results in a giant step, it will be shown in section 4.3.5 that this step gathering results in facet planes inclined by $\pm 18°$ with respect to the surface normal. This points to a larger influence of diffusion gradients related to the equilibrium morphology than can be inferred from the material transport in the images of figure 4.12. By waiting sufficiently long, the characteristic morphology as depicted in figure 4.12 (h) evolves.

Very similar to the process just described is the morphological evolution upon slowly cooling the sample through the transition temperature of 660 °C. Again, the smooth steps are subject to surface as well as bulk diffusion thus rapidly moving across the surface and losing their straight shape. In figure 4.13 (a) one of the bulk channels imposing these large diffusion gradients on the surface is imaged. Its size is falsified by the defocus condition, which was chosen such as to visualize the steps. Clearly, there is a material (atoms or vacancies) flux away from this channel, while the steps in the rest of the image move in the opposite direction. In figure 4.13 (d) all steps are already roughened due to reduced surface diffusion perpendicular to the periodic axis. Consider the steps related to the bulk channel in the picture and moving from right to left: They lose their straight shape, which is accompanied by less step motion in the middle of the inlet, while the steps at the border still proceed quickly towards the left. This results in four separate

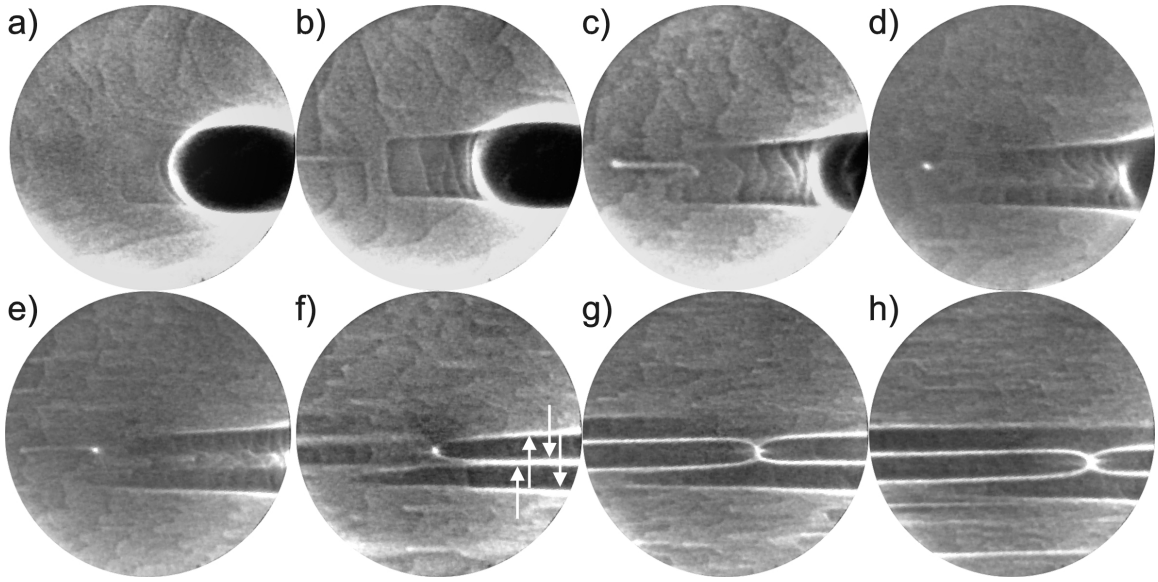

Figure 4.13: Observation of the facet construction on the $(001\bar{1}0)$-surface upon cooling slowly from 685 °C to 617 °C. The arrows in (f) point to slopes in the morphology, which evolve into facets. Oppositely directed arrows point to opposite slope with respect to the surface. The MEM images comprise a field of view of 6.7μm, with the periodic axis of the sample coinciding with the images' horizontal.

accumulations of steps perpendicular to the motion direction, as indicated by arrows in figure 4.13(f) (oppositely directed arrows point to opposite slopes). Theses slopes will be shown to be facet planes rather than any arbitrary accumulation of steps, indicating that the equilibrium morphology indeed influences the diffusion. The gradients of the bulk channels only accelerate the diffusion parallel to the periodic direction of the sample.

A similar structure is built up from the other side of the image. While its lower trench would adjoin the upper one of the described construction, there is a defect to separate the two. Both outer trenches continue their way to finally form a structure with six facet planes (figure 4.13(h)), whose width can be estimated to be 0.5 μm, while their elongation is larger than the image size.

Facet Dissipation

The facet dissipation can be followed by heating the sample through the phase transition of 660 °C as illustrated by a series of MEM images in figure 4.14. While there are a number of ridges visible in part (a) of the figure, these vanish one after another during heating. Again, the bulk channels (located on the left hand side outside the images) impose a gradient on the

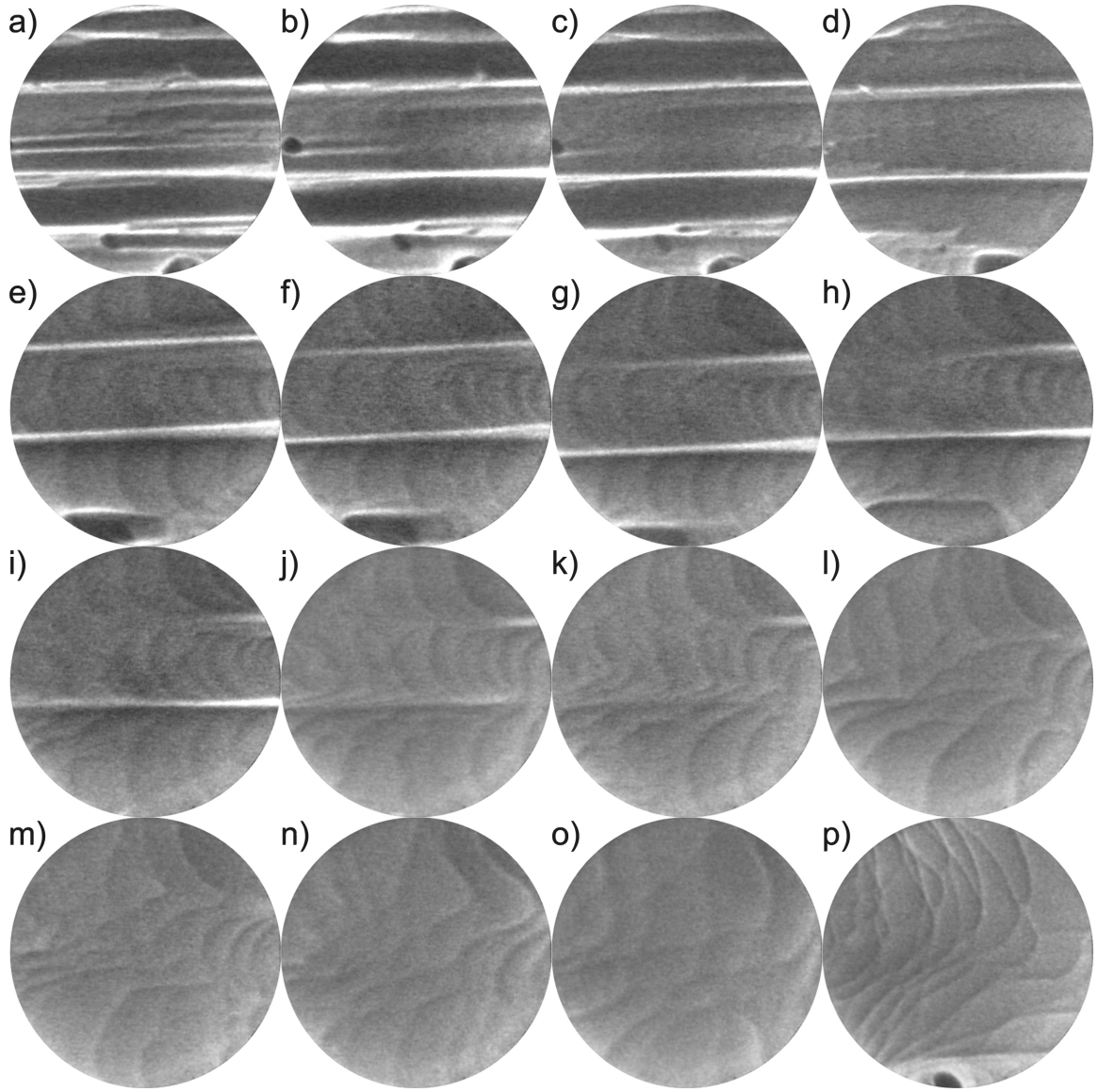

Figure 4.14: A series of MEM images of the twofold $(001\bar{1}0)$ surface during facet dissipation. The diameter of the sections is 6.7 μm, the periodic axis of the sample is aligned with the images' horizontal, the investigated temperature range is 617 °C to 682 °C in a time frame of 18 min. The time separation between consecutive images is not equal.

surface diffusion, which is responsible for a large amount of step motion. At the same time there are gradients to reach the equilibrium morphology independent of the bulk.

While 4.14 (a-d) show a large number of steps responsible for the removal of several facet planes, the precise step movement actually leading to the facet dissipation can more easily be understood towards the end of this series, when only two rather flat ridges remain. The

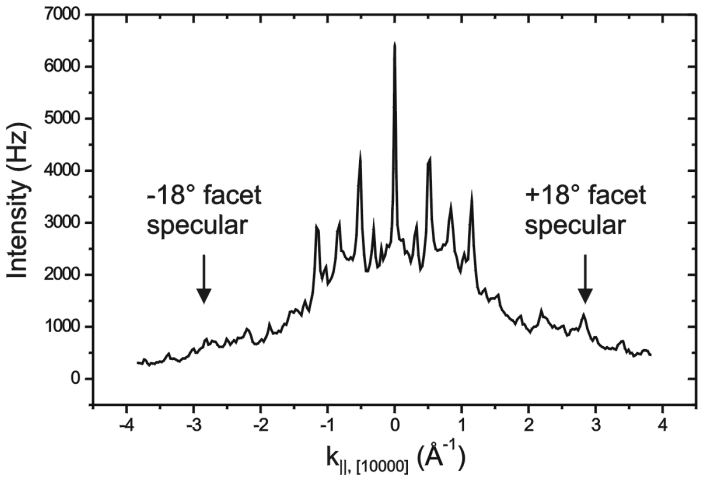

Figure 4.15: Helium atom diffraction from the $(001\bar{1}0)$-surface at room temperature with a beam energy of 21.6 meV. Spectra recorded at varying energy indicate a movement of the labeled diffraction spot in **k**-space. These peaks are the speculars of the facets, found at an inclination angle of $\pm 18\,^{\circ}$. As the spectrum was taken in a different set-up, the cooling rate is difficult to compare to the MEM data. From the rather low intensity of the specular (and even lower intensity of higher order facet reflections) a medium cooling rate with respect to figure 4.11 is inferred.

remaining steps in the pictures are all moving to the left, caused by the influence of a bulk channel at the left hand side outside the image. At temperatures above 660 °C diffusion along the step edges becomes possible in addition to the diffusion along the periodic axis, as can be inferred from the steps' smooth shape. This is very important for the dissipation mechanism, as it straightens the steps, which are U-shaped. (They are aligned with one facet plane, bend to be perpendicular to the facets, and again bend to contribute to the next facet plane.) Atoms forming the facet step can thus diffuse along the step to the middle of the U-shape, eventually leading to a straight step. The facet is completely dissipated once all steps are straightened.

4.3.5 Facet Structure

It has been explained in the previous section that the bright stripes and darker areas in the MEM images are a one-dimensional hill-and-valley morphology perpendicular to the periodic axis of the sample and this is not an arbitrary accumulation of steps, but facet planes inclined at a specific angle to the surface. This is shown in the following.

LEED patterns of such a morphology exhibit diffraction spots moving with varying energy along the quasiperiodic (10000)-direction. Hence, these spots arise from the diffraction of one-dimensional facets inclined perpendicular to the periodic direction. In order to determine the

inclination angle and structure of the facets, Helium scattering spectra were recorded along the quasiperiodic direction. Since these were taken in a different machine, the cooling rate is not directly comparable. That facets have been formed is revealed by the specular diffraction spots of the facets labeled by arrows in figure 4.15. These appear at $\pm 18^\circ$ off the specular from the macroscopic surface independent of the He beam energy. Due to the low intensity of diffraction spots from the facet planes, it is difficult to determine the structure of the facets. However, at $\pm 18^\circ$ off the sample normal (10000)-equivalent planes are located, which were indeed found to form facet planes on $Al_{71.8}Ni_{14.8}Co_{13.4}(001\bar{1}0)$ surface at room temperature [76]. Consequently, the surface free energy of the (10000)-orientation is lower with respect to the $(001\bar{1}0)$-plane in the low temperature phase.

4.4 The Phase Transition between the Modifications Type I and S1

Since the reversible faceting transition on d-Al-Ni-Co$(001\bar{1}0)$ and the smoothing transition on the twofold (10000)- and the tenfold (00001)-sample orientation are connected to a strong material exchange between bulk and surface, the surface phase transitions are clearly related to a bulk transition. The extrapolation of the phase diagram in figure 4.1 yields a bulk structural transition from the type I decagonal modification to the S1 modification near the observed morphological transition temperature. While it is impossible to determine the direction of mass transport, (i.e., into the bulk or out of the bulk), from the MEM data presented here, positron annihilation studies reveal an increase in structural vacancies for crossing this phase transition from lower temperatures [99]. Based on that study it can be concluded that atoms diffuse from the surface into the bulk upon cooling and out of the bulk to the surface upon heating from type I to S1. Regarding the facet formation this implies the trenches to be preferentially dug into the surface.

4.4.1 Facet Formation on Quasicrystal Surfaces

Having analyzed the facet formation and dissipation as well as its structure, it remains to resolve why these facets are energetically favored at low temperatures and why they are not stable at high temperatures. Generally, the equilibrium morphology of a crystal is determined by the lowest possible surface free energy. Atomic planes of low surface free energy correspond, to a first approximation, to densely packed net planes exhibiting strong attractive interactions between their atoms. Assigning the corresponding Miller indices to each net plane, the atomic density is in most cases larger for smaller indices. Consequently, the surface free energy scales with the indices and planes associated to small indices dominate the morphology.

In quasicrystals, there are short reciprocal lattice vectors in infinitely many directions, thus indicating the possible formation of a large number of facet orientations. However, to many such vectors no densely packed atomic plane corresponds. Instead, one hint about the morphological importance of the net planes is given by the structure factor and consequently by the intensity of the corresponding Bragg peak in diffraction patterns. Strong Bragg reflections reveal high density atomic net planes, a property which has been elucidated by Steurer and Cervellino [100]. From the diffraction pattern in figure 2.8 (a) a good candidate for a high density atomic net plane is the (10000) reflection, which corresponds to a plane running parallel to the tenfold axis and inclined by $\pm 18°$ off the horizontal (and its tenfold rotational equivalents) of figure 4.16. One set of cuts of those planes with the quasicrystalline plane are the densely packed atomic rows indicated by blue lines. The shortest bonds in the quasicrystalline planes amount to 2.43 Å and lie on the just described rows, while the nearest neighbor distance between atoms in adjacent quasicrystalline planes yields 2.52 Å [100]. Together, these indicate the formation of the strongest bond planes and therefore low surface free energy net planes. Quantitatively, the densest planes perpendicular to the $(001\bar{1}0)$-surface normal contain about 17 % less atoms than these inclined net planes. A buckling of 0.25 Å was allowed for the (10000)-planes, while the $(001\bar{1}0)$-planes are almost flat.

Having illustrated the importance of dense atomic planes for the surface morphology and their association to strong Bragg reflections, a qualitative Wulff plot, which illustrates the surface free energy as a function of surface normal vector, for this quasicrystal can be constructed: The deepest cusps will be found at normal vectors parallel to short reciprocal lattice vectors associated to high intensity Bragg points. For the two-dimensional cut along the decagonal plane, this means deep cusps at (10000)-equivalent directions and shallower cusps along $(001\bar{1}0)$-equivalent directions, as illustrated in figure 4.17. The equilibrium shape is then determined by the inner envelope of planes perpendicular to and passing through the radius vector of the Wulff construction.

Thus the (10000)-equivalent facets are energetically favored, but their vanishing at high temperature is still not resolved and is discussed in the following. As the temperature increases, the step free energy usually decreases and accordingly the corresponding cusps in the Wulff plot become less and less pronounced. Hence, the dissipation of the (10000)-facets might be attributed to temperature effects alone, without any structural change. To rule out this effect, total step and surface free energy values would have to be known, which cannot be derived from these experiments. However, the coincidence of the faceting transition with a bulk structural transformation suggests that other factors dominate. Moreover, additional investigations on a sample of different composition ($Al_{71.8}Ni_{14.8}Co_{13.4}$) whose type I $\leftrightarrow$ S1 phase transition occurs at

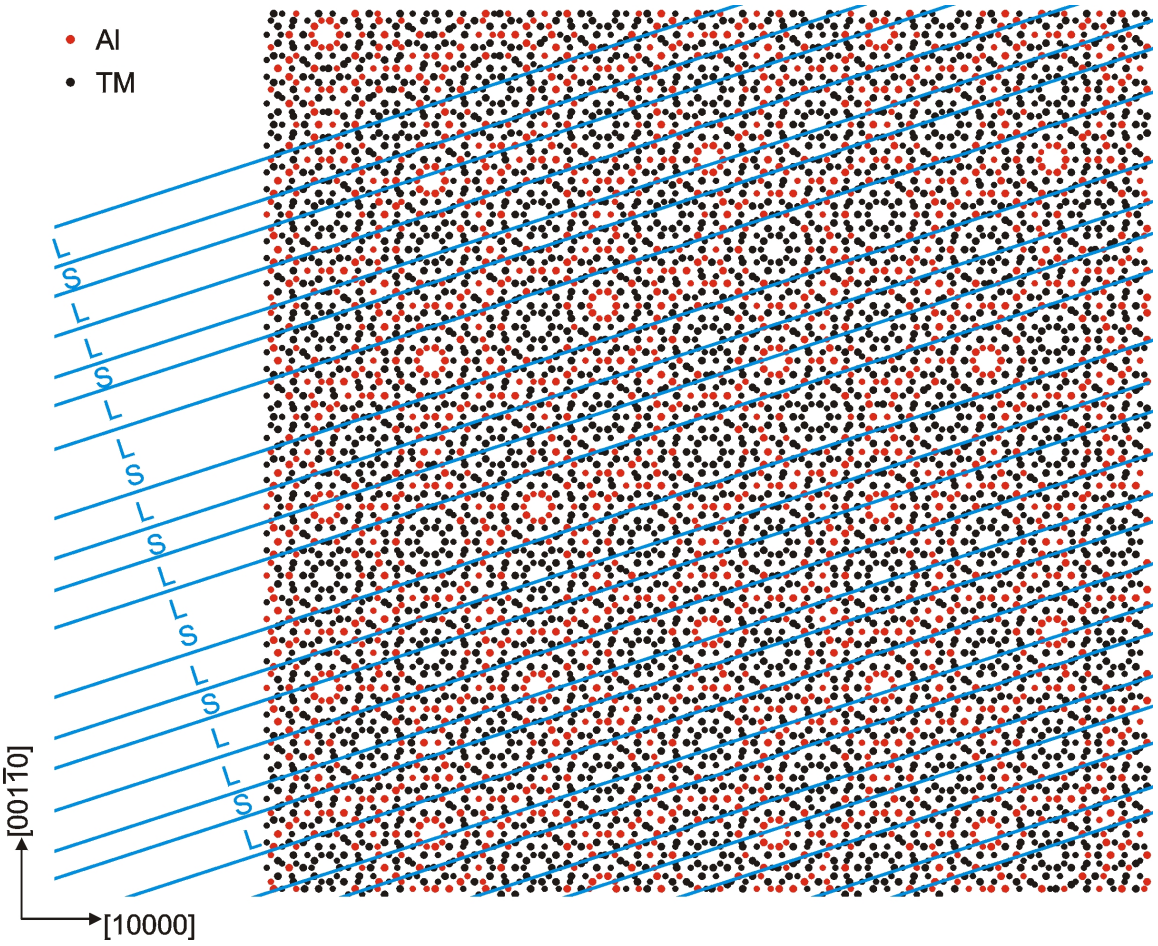

Figure 4.16: Atomic structure in the tenfold plane in the model after Yamamoto and Weber [32, 101]. The blue grid indicates densely spaced atomic rows. These are inclined by 18 ° from the surface normal and thus correspond to a (10000)-orientation. The spacing follows a Fibonacci sequence with S = 4.5 Å and L = τS = 7.2 Å.

a higher temperature also shows this faceting transition at a higher temperature, namely at the bulk transformation temperature. This strongly suggests a close relation to the structural phase transition. In the following the structural changes in the bulk transformation are discussed in order to determine the possible reasons for a change in surface free energy.

4.4.2 The Effect of Structural Changes on the Faceting Transition

Figure 4.16 illustrated that dense atomic rows within the quasicrystalline plane can be found inclined by ±18° with respect the (00$1\bar{1}$0)-surface plane. While previously these were found by a combination of reciprocal space considerations and atomic bond length, one can now characterize

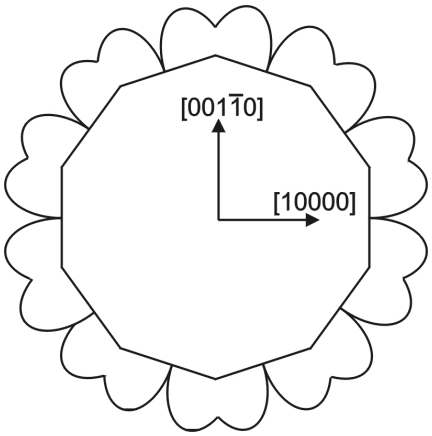

Figure 4.17: Wulff plot of the quasicrystalline d-Al-Ni-Co plane. The inner decagon describes the equilibrium crystal shape.

these rows by the tiling covering the quasicrystalline plane and the atomic clusters decorating its vertices. Superimposing an ideal rhombic Penrose tiling on the atomic structure as illustrated in figure 4.18, one realizes that the rows of high atomic density (blue lines) are aligned parallel to edges of the rhombic tiles. These rows can be found at two specific distances of $r = 2.35\,\text{Å}$ and $r = 6.15\,\text{Å}$ to the tiling's vertices, as indicated in figure 4.19 (a). Hence, to find dense atomic planes perpendicular to the quasicrystalline plane, the underlying tiling convoluted with the cluster can be considered. The few atoms in the gaps between the clusters can be neglected in the discussion of the net planes.

The basis for the success of this concept is the discrete spacing of vertices perpendicular to the [10000]-, and [001$\bar{1}$0]-direction. The model used in figure 4.18 corresponds to an ideal rhombic tiling, while it is generally accepted that the type I structure exhibits a random rhombic tiling. To evaluate if this induces changes in the determination of densely packed rows the derivation of a random tiling from an ideal one is considered. As indicated in figure 4.19 a phason flip always occurs along one of the [001$\bar{1}$0]-equivalent directions, i.e., parallel to the tile edges. Each jump always results in the cluster center to appear on lines which are already occupied by cluster centers, and the change in number of vertices on different lines is canceled out. Hence, the introduction of randomness does not change the overall distribution of cluster centers relative to the net planes. The same is also true for the occupation lines inclined by $\pm 18°$. Consequently, high density net planes are found at the same positions in an ideal and random rhombic tiling.

Now, from a comparison of the net planes, a 17 % higher density is found in (10000)-planes than in the densest (001$\bar{1}$0)-planes, revealing the lower surface free energy of the facet planes. A buckling of 0.25 Å has been allowed in this estimation.

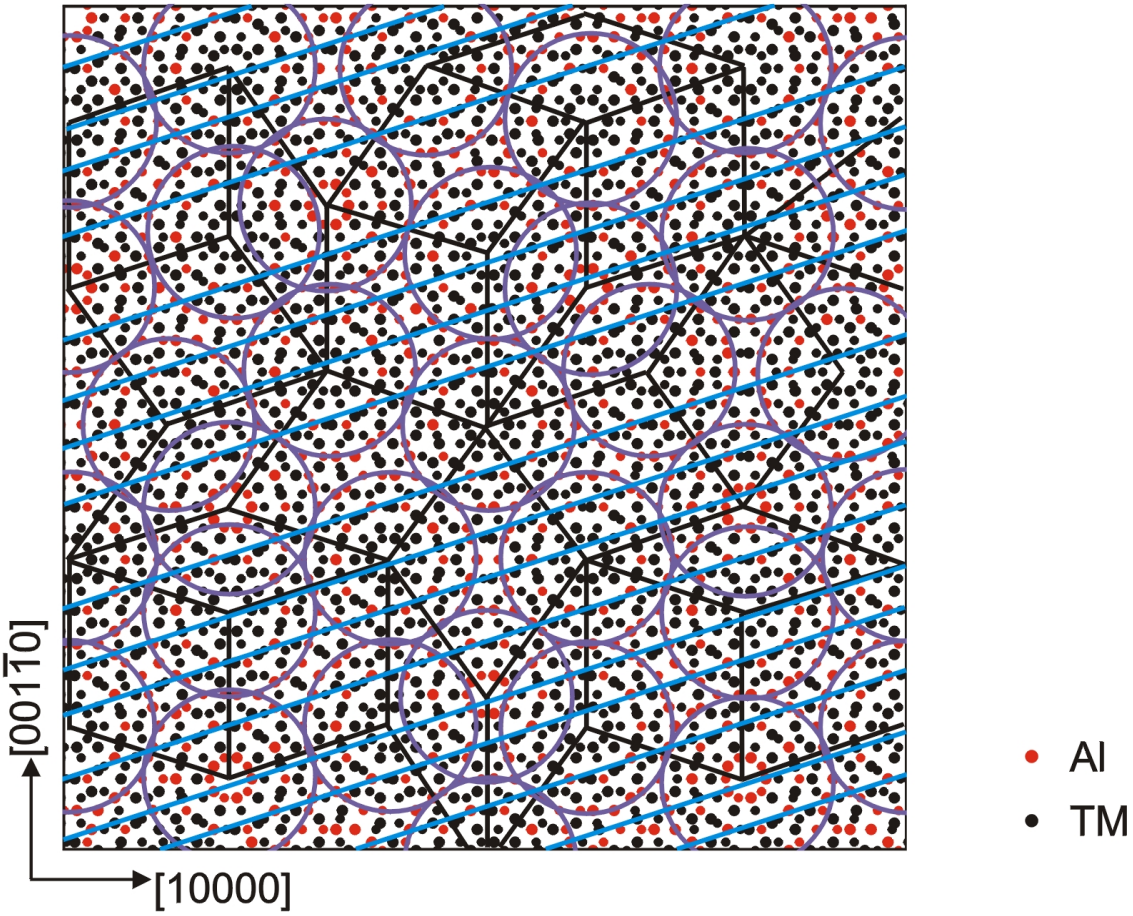

Figure 4.18: Atomic structure (100 Å x 100 Å) in the tenfold plane viewed in the tiling-cluster model. The red and black dots indicate Al and transition metal atoms, respectively. Superimposed is an ideal rhombic Penrose tiling (black) of edge length 19.78 Å, with the clusters marked by purple circles. The blue grid indicates densely spaced atomic rows inclined by 18 ° with respect to the (00$1\bar{1}$0)-surface normal, thus corresponding to a (10000)-orientation. The spacing follows a Fibonacci sequence with S = 4.5 Å and L = τS = 7.2 Å.

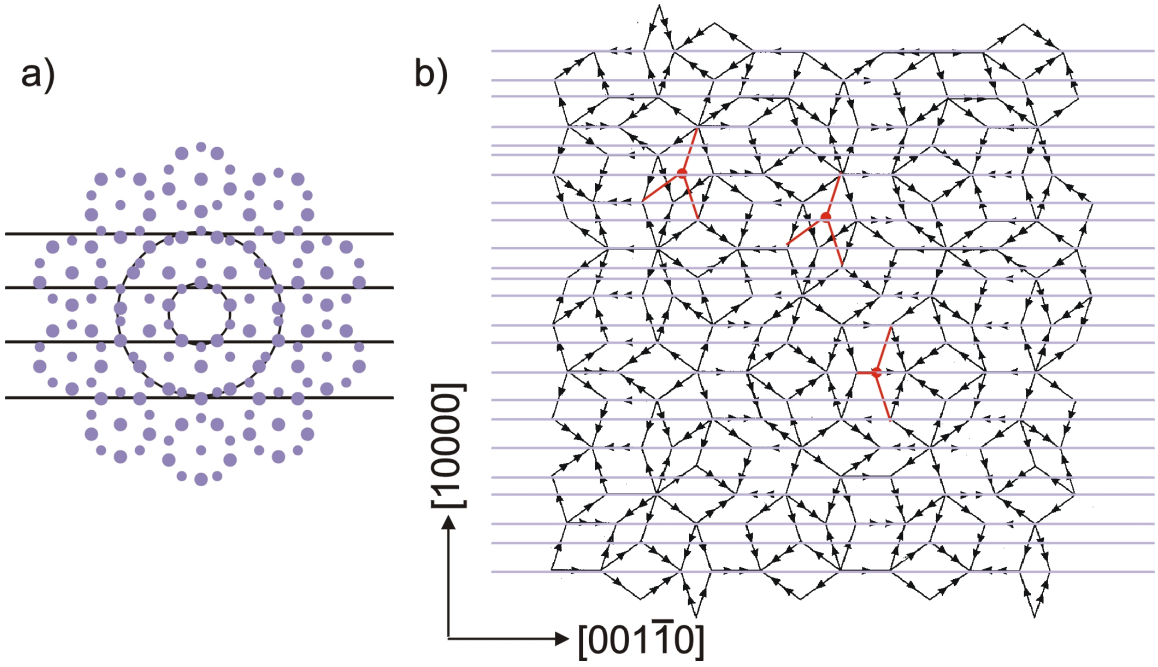

Figure 4.19: (a) Atomic cluster with one set of high density atomic rows (at a distance of $r = 2.35\,\text{Å}$ and $r = 6.15\,\text{Å}$ from the cluster center) and (b) rhombic tiling and lines containing its vertices. (Note that the (10000)-plane is now oriented as the surface plane. The red circles exemplify phason flips to introduce randomness into the ideal tiling, the red lines are the new tile edges after the flip.

The same has been carried out for a pentagonal tiling, in which a difference of 12 % has been found for the respective planes. Hence, the (10000)-planes are still expected to exhibit a lower surface free energy than the (001$\bar{1}$0)-planes. Since the growth faces are the (10000)-planes, a lower surface free energy of the (10000)-planes is indeed expected [5]. However, the 12 % increased atomic density is consequently not sufficient to compensate a 5 % enlarged surface area at high temperatures.

4.4.3 (10000)-Surface Termination

Implicitly, the step-terrace morphology of the (10000)-surface orientation has already been discussed in the previous sections. In section 4.4.1 high density atomic planes have been identified perpendicular to (10000)-equivalent axes. These are possible low surface free energy terminations. Structurally similar planes have been marked by blue lines in figure 4.16. Their spacing amounts to $S = 4.5\,\text{Å}$ and $L = \tau S = 7.2\,\text{Å}$, arranged in a Fibonacci sequence. Step heights of $8 \pm 0.4\,\text{Å}$ and of $5 \pm 0.4\,\text{Å}$ have been found in room temperature STM investigations [11], thus

roughly matching the model.

4.4.4 Low Temperature Equilibrium Morphology

Finally, the question remains, why all three surfaces show a high step density at low temperatures, i.e., in the type I phase, in contrast to the large terraces observed above the phase transition. In view of this discussion it first needs to be considered if the rough surface morphology below 650 °C is in equilibrium. Possibly, the phase transition and its related immense material transport upon cooling have left their 'traces'. The experimental approach to solve this question is to keep the surface at a temperature just below this transition. Therefore the sample was held at about 600 °C for 12 hours. After this time period the surface still exhibits a similar roughness.

In order to estimate the time necessary to reach equilibrium, the facet formation in figure 4.12 is again considered. There, after an interval of 45 minutes the morphology is already significantly changed, but the steps are not yet in their equilibrium shape. Instead, they are still slowly moving under the influence of a gradient along the periodic direction. Recalling that the surface diffusion along a quasicrystalline direction was found to be significantly reduced with respect to the periodic direction, the observed surface can be assumed to be far from equilibrium. Therefore, it is unlikely that 12 hours are sufficient to reach a fully equilibrated surface.

Calculations have shown that significant bulk Al diffusion is only observable above 60 % of the melting temperature, i.e., 600 °C, with a mean square displacement of $3 \times 10^{-3} \mu m^2/s$ and $12 \times 10^{-3} \mu m^2/s$ at 700 °C along the quasicrystalline and periodic direction, respectively [102]. Experimentally, the bulk diffusion coefficients for Ni and Co have been determined to $D_{Ni} = 10^{-15} m^2/s$ and $D_{Co} = 10^{-17} m^2/s$ at 600 °C [103]. Within 12 hours Co atoms therefore undergo a mean displacement of $\bar{x} = \sqrt{Dt} = 0.66\,\mu$m. Surface diffusion might be limited by additional factors. For example the material exchange with the bulk might lead to a very small change in stoichiometry at the surface. Adatoms decorated at step edges could then significantly lower the surface diffusion. This would explain the drastic change in diffusivity with the phase transition. Consequently, the equilibrium morphology of the low temperature phase cannot be obtained in a reasonable time interval.

4.5 The Phase Transition S1 ↔ Basic Ni

An additional surface phase transition can be found at about 730°C on both twofold (10000)- and (001$\bar{1}$0)-surfaces. This transition can also be related to a structural bulk transition, namely to the transformation between the S1 and basic Ni modifications. First, the observations on the

(10000)-sample are analyzed, then those of the $(001\bar{1}0)$-surface. Finally, an argument is given, why no observable changes are expected on the tenfold (00001)-surface.

4.5.1 The Phase Transition on the (10000)-Surface

For the characterization of the transition a series of MEM images is shown in figure 4.20. The depicted transition is recorded while quickly changing the sample temperature from 730 °C to 700 °C and vice versa.

At the beginning a number of steps can be observed, which separate planes of identical intensity. Upon cooling two new sets of planes of different intensity appear. Their intensities are significantly larger than those of the original planes and slightly different with respect to each other. Figure 4.21 illustrates the top view onto the surface. Same colors indicate equivalent intensity in the data. The original planes are blue, separated by black steps. The new planes are colored green and red. Both start spreading from original step edges across the terraces, as can be inferred from figure 4.20(b-d) and illustrated in 4.21(b), until they eventually meet and the original (blue) surface is not visible any more (figure 4.20(e) and 4.21(c)). Now, one of those terminations continues spreading while the other type is displaced as shown in figure 4.20(f-h) and figure 4.21(d). Finally, this dominant termination covers the whole surface (figure 4.20(h) and figure 4.21(e)). The surface phase transition is now completed.

Heating through the transition is shown in the remainder of figures 4.20 and 4.21. Again, new terminations appear at the step edges and spread across the terraces. Their intensity equals the two previously observed, as indicated by their colors in figure 4.21(g). When they coincide, one termination continues to spread in its direction by replacing the other one, until the surface exhibits equivalent terraces only. The intensity of the final termination is the same as at the very beginning, i.e., as in figure 4.20(a) and indicated in figure 4.21(a). Consequently, this surface phase transition is reversible.

The cycle just described is observed if the sample temperature is changed relatively quickly, while a very slow variation would allow the equilibration of the surface at all temperatures. The transition can then be separated into two parts, each one reversible. The process is illustrated in figure 4.22.

The starting point is again the ‘blue’ termination on all terraces. Cooling slowly induces only one set of planes of larger intensity to appear at the step edges. These slowly evolve to cover the whole terraces as indicated in figure 4.22(b-c). This termination is an equilibrium termination in a very narrow temperature range of about 20 °C. Further cooling results in the termination of slightly higher intensity to appear at the step edges and to spread over the terraces to finally completely form the termination. Heating the sample now reverses the process. First the red

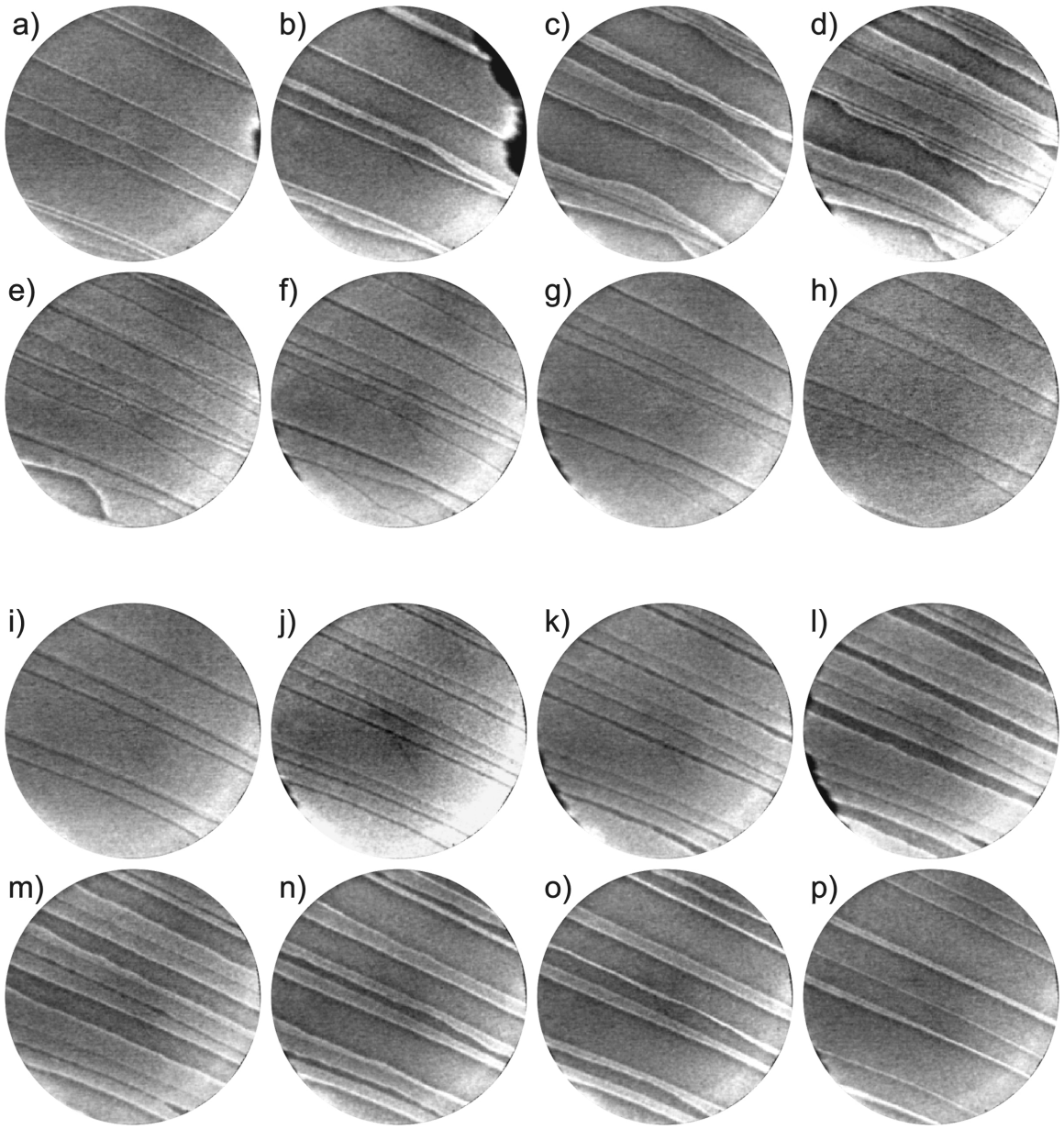

Figure 4.20: A series of MEM images upon sweeping through the phase transition S1 ↔ basic Ni on the twofold (10000) d-$Al_{72.3}Ni_{18.2}Co_{9.5}$. Images (a)-(h) are successively recorded during sample cooling, while (i)-(p) are subsequently taken upon heating through the same temperature range, each direction in a time interval of about 2 min. The images are 6.7 μm in diameter. The black borders in some images, are due to the edge of the illuminating electron beam.

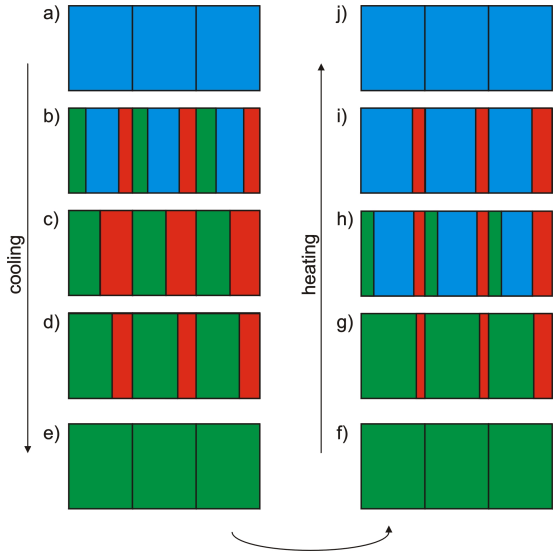

Figure 4.21: Schematic top view onto the surface during the phase transition S1 ↔ basic Ni on the twofold (10000) d-$Al_{72.3}Ni_{18.2}Co_{9.5}$. Different colors indicate different intensity in the MEM data. However, the original step edges do not necessarily remain at the same place.

labeled planes appear at the step edges and spread over the terraces before the final termination evolves. Hence, the termination before and after the transition are the same, no matter if the sample temperature is slowly or rapidly changed, as is expected for equilibrium states.

Terminations

In MEM mode, in which these images were recorded, the major part of the electrons is reflected in front of the surface. The contrast on the terraces is due to a difference in work function of the respective terminations as has been explained in chapter 3. Hence, the three different intensities correspond to three terminations of different work function. The darkest imaged terminations thereby exhibit the smallest work function, while planes of higher intensity are associated with larger work functions. Related to the schematics, this implies a small work function for the blue terminations, while red and green planes exhibit considerably larger work functions.

A difference in work function is expected for planes of varying atomic density with the same stoichiometry and for planes of different stoichiometry. For example, Al possesses a work function of 4.41 eV, 4.06 eV, and 4.24 eV for (100), (110), and (111) surface orientation, respectively. The value for the polycrystalline material is 4.28 eV. The work function of polycrystalline Co was measured to be 5.00 eV and for Ni 5.15 eV [104]. Consequently, Al-rich planes exhibit a smaller work function than those of higher transition metal content. Moreover, a larger change in

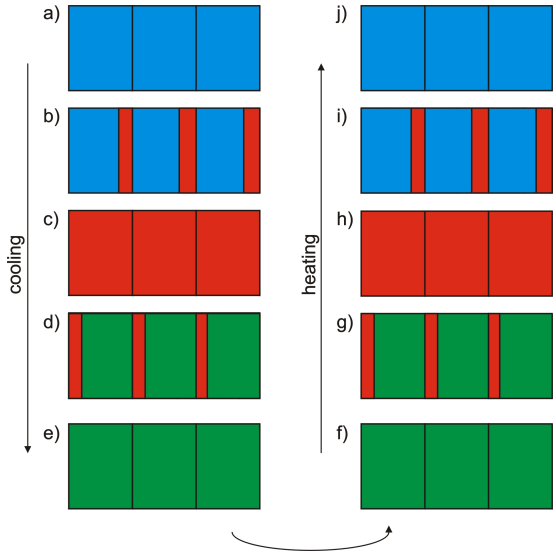

Figure 4.22: Schematic top view onto the surface during the phase transition S1 ↔ basic Ni on the twofold (10000) d-$Al_{72.3}Ni_{18.2}Co_{9.5}$. Different colors indicate different intensity in the MEM data. The original step edges do not necessarily remain in the same place. In contrast to figure 4.21, the sample temperature was very slowly varied.

work function can be assumed for chemically different planes than for planes of varying density. Therefore, it may be concluded that the high temperature basic Ni termination with the smallest work function is more Al rich than the termination of the S1 phase.

While the work functions of the 'green' and 'red' termination are very similar, bright field LEEM images are used to estimate the degree of structural difference as revealed by the LEED structure factor. In order to observe the three different terminations simultaneously, the sample temperature was quickly decreased. Figure 4.23, corresponding to figure 4.20 (c) and figure 4.21 (b), then shows phase contrast between the three terminations and therefore indicates a considerable difference in structure factor. In order to determine the structure of the termination in more detail the analysis of the LEED intensity as a function of energy of more diffraction spots in a large energy range would be necessary.

Mechanism of the Surface Phase Transition

For a more detailed description of this phase transition, the step motion associated with the spreading of the planes as described in the previous section is considered in the following. While figures 4.21 and 4.22 represent the observations which are directly accessible by LEEM, figure 4.24 is an interpreted step scheme of the encountered situation. It should be noted that both

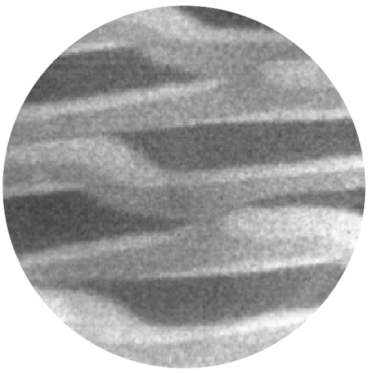

Figure 4.23: Bright field LEEM image during the phase transition S1 ↔ basic Ni. The sample temperature was quickly varied in order to observe the three terminations simultaneously. This image was recorded on a different sample position than figure 4.20. Here, the steps are not all parallel. The field of view is 6.7 μm.

the step directions as well as their heights are unknown. Consequently, the thickness of the colored layers was arbitrarily chosen. However, these assumptions do not qualitatively change the following interpretation. A difference in step heights would only change the amount of step motion, which is not quantitatively measured anyway.

First, the phase transition upon slowly cooling is analyzed as this represents the equilibrium. The starting point is a step-terrace structure with structurally equivalent planes as indicated by blue bars in figure 4.24. The appearance of a new termination at step edges can be explained by atoms of the outermost planes being removed, thereby exposing underlying planes. The removed atoms are added at high steps. Thereby a minor movement of these steps is induced as indicated by their displacement from the dotted lines in figure 4.24. Likewise, one complete layer can be removed from the terraces to yield a new step-terrace morphology with different termination. The temperature range in which this termination is in equilibrium is very narrow, approximately 20 °C. Further cooling the sample results in another change of the termination. This time, a new layer is created by removing atoms from high step edges and adding them on the terraces. Since the new layers are structurally different from the original blue ones, as discussed in the previous section, the added layers must either contain the blue planes or be a part of them. The first case was chosen to be depicted in figure 4.24. However, the other option would only result in a smaller movement of the high steps. Heating through the phase transition reverses this process.

If the sample temperature is quickly varied when going through this phase transition, the intermediate equilibrium termination, i.e., the 'red' termination, is not reached. Instead, the two parts of the slow process overlap. The corresponding step schematic is shown in figure 4.24

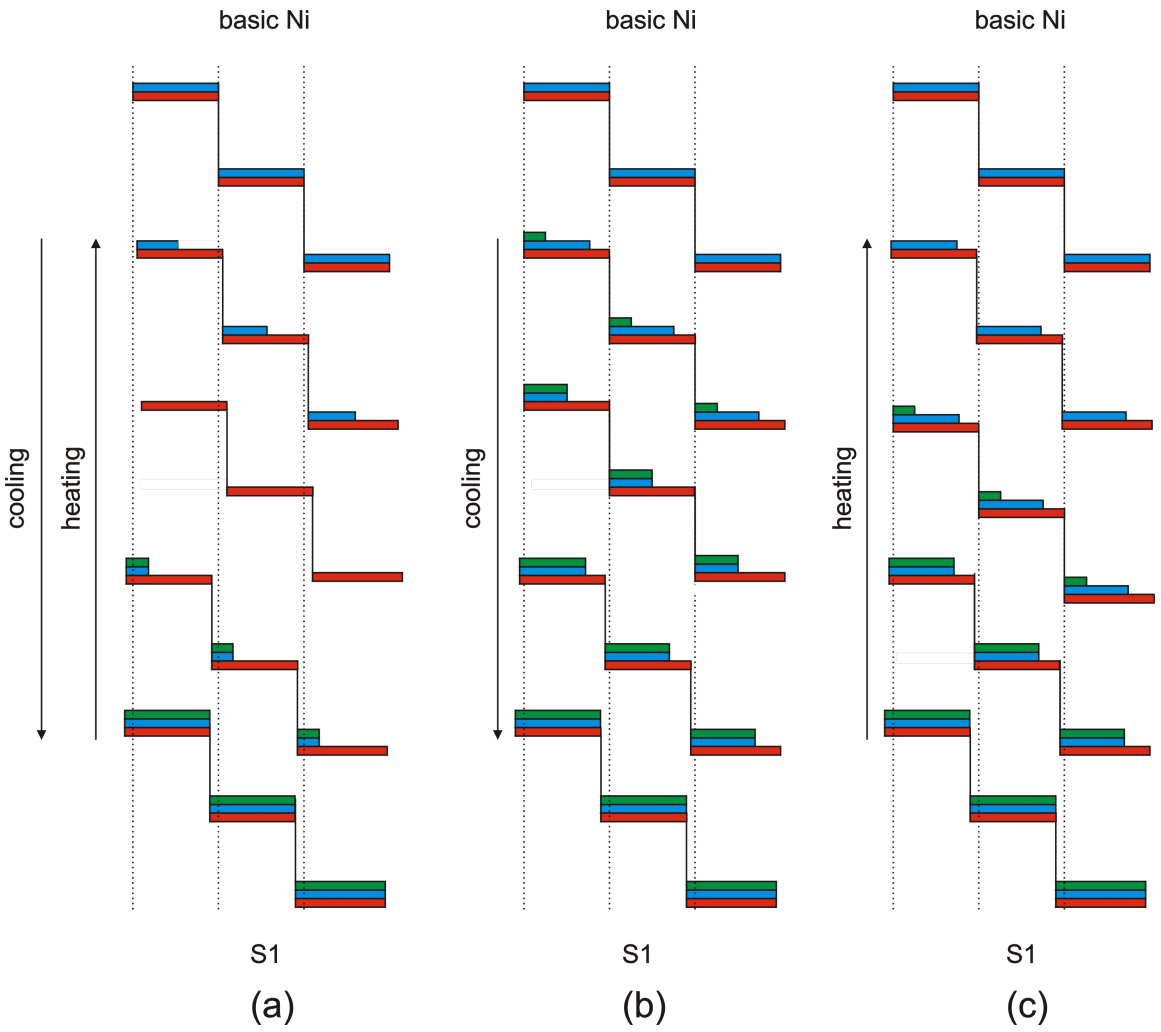

Figure 4.24: Schematic step motion during the phase transition S1 ↔ basic Ni on twofold d-$Al_{72.3}Ni_{18.2}Co_{9.5}$(10000). Different colors indicate different intensity in the MEM data, as introduced in figures 4.21 and 4.22. (a) shows the transition when slowly varying the sample temperature, while (b) and (c) illustrate fast cooling and fast heating, respectively.

(b) and (c) for cooling and heating, respectively.

The motion of the large steps is very difficult to image by LEEM. If their heights are large with respect to the material being added or removed, their motion is indistinguishable from the thermal drift in the images. For example, if one atomic layer is removed from a terrace of 0.5 μm width, this results in a shift of about 0.16 μm of an 8 Å high step.

While the observations can thus be fully explained by a surface phase transition alone, there might again be a material exchange with the bulk. Hence, the steps might additionally be shifted by serving as a sink or source for atoms of the bulk. Clearly, this effect cannot be distinguished from a thermal drift if the amount of material is relatively small. It has been suggested by positron annihilation experiments that the basic Ni phase exhibits less structural vacancies than the S1 phase, but no quantitative data is available yet [105].

Mechanism of the Surface Reconstruction

It has been shown in the previous sections that the surface undergoes a phase transition by changing its termination. By an estimation of the difference in work function it has been argued that at very high temperature the surface consists of planes being more Al-rich than the termination at lower temperatures.

While the complete phase transition can be reconciled with the structural bulk phase transition basic Ni ↔ S1, the existence of an intermediate equilibrium state is not know from the bulk. Therefore, this might be attributed to a surface phase which occurs as an intermediate phase during the phase transition.

In order to understand the possible reasons for the change in termination, the structural model of the surface is investigated. The atomic structure of the basic Ni phase is obtained by decorating the vertices of a pentagonal tiling with atomic clusters (a section is depicted in figure 4.25). This method leaves some gaps in the tenfold plane, which can be ignored for the purpose of this analysis, since it was shown in section 4.4.2 that the densest planes consist mostly of atoms on the tenfold substructures within the cluster. A possible termination is indicated by the black line in the middle. It is of high atomic density and consists of both Al and transition metal atoms.

The structural phase transition between the modifications basic Ni and S1 implies a change of the corresponding tilings from ideal pentagonal to random pentagonal. A tiling is transformed by phason flips of its vertices. Since the vertices are decorated by atom clusters, this involves a multitude of atomic flips. Single atomic flips have recently been observed by Abe et al. [35]. Although their investigations were focused on the vibrational properties of atomic jumps, these are the same that occur in the phase transition. The findings confirm jumps into structural

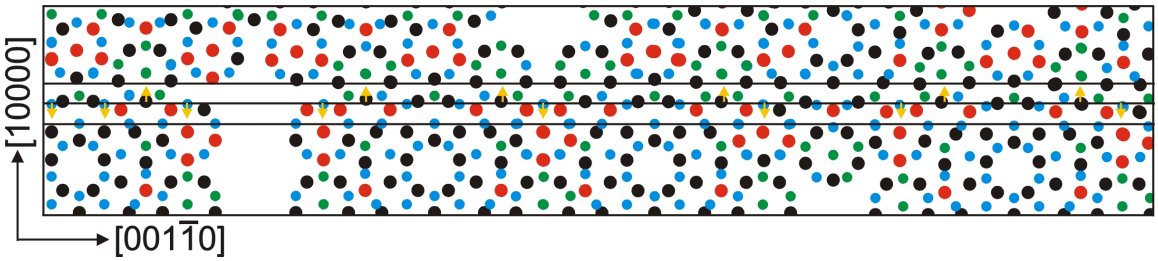

Figure 4.25: Structural model of the (10000)-surface. The middle black line indicates a densely packed atomic plane of mixed chemical composition, a possible surface termination of the basic Ni phase. Initial atom flips of the basic Ni → S1 transition are marked by orange arrows. These result in a decrease of the atomic density in the original termination and in an increase of the density of the TM rich underlying plane.

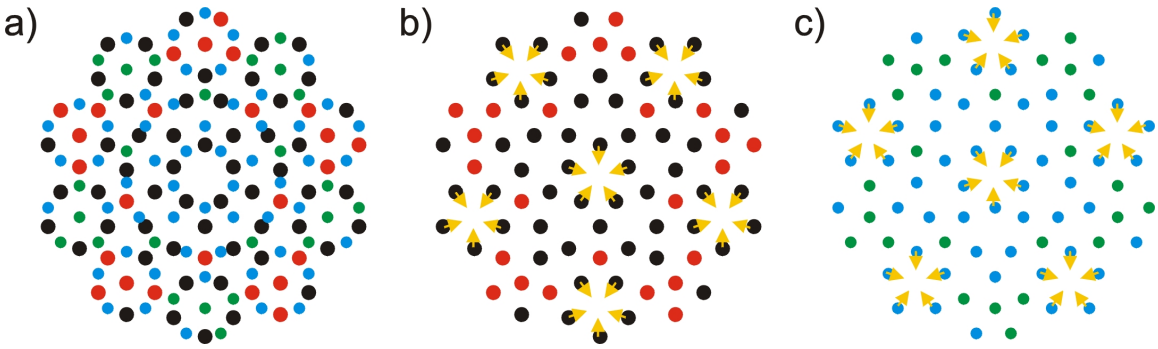

Figure 4.26: Cluster model for d-Al-Ni-Co in the model from Yamamoto and Weber [32]. (a) two layers of the cluster, where red and black indicate Al and transition metal atoms in the first layer, respectively, green and blue denote Al and transition metal atoms in the second layer. (b) and (c) picture the first and second layer separately. The arrows point to initially possible atom jumps into structural half-vacancies. (Only one of the five jumps within the pentagonal substructures is allowed.)

half-vacancies by 0.95 Å from the original position as illustrated in figure 4.26. Therefore, all jumps are directed along [10000]-equivalent axes, i.e., perpendicular to the surface, and 36° off normal.

The arrows in figure 4.25 indicate possible atomic flips at the beginning of the phase transition basic Ni →S1. If the middle black line is considered to be the surface termination due to its high atomic density, a number of atoms can jump out of this plane by 0.95 Å. As a result the surface exhibits an increased buckling. This reconstruction is unlikely to be sufficient to induce the observed phase contrast, since the stoichiometry is not changed. In contrast, incorporating the jumped atoms in the adjacent, transition metal rich planes, considerably increases their density.

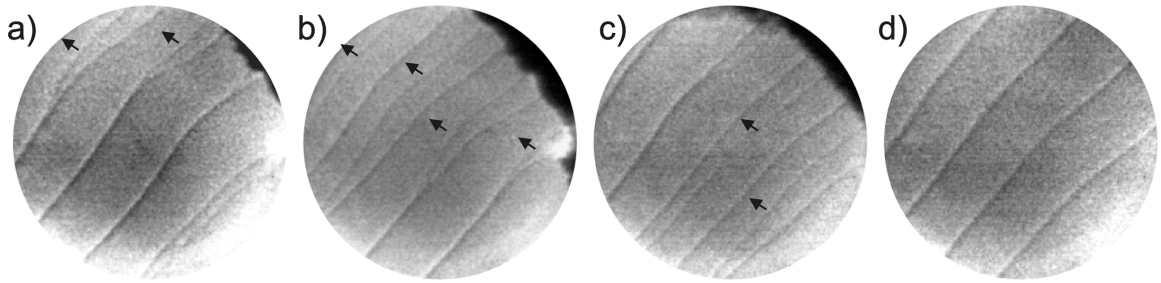

Figure 4.27: The phase transition basic Ni → S1 on the $(001\bar{1}0)$-surface. All steps split into two, one of which is moving through the neighboring terrace. The direction is indicated by arrows. A second step movement of this kind follows. The field of view is 6.7μm. (The black borders in (a-c) are due to the edge of the illuminating electron beam.

This might decrease their surface free energy and ultimately favor one of these to constitute the termination, thus leading to a topographic step movement. The newly exposed plane is then rich in transition metal atoms, leading to a larger work function in agreement with the MEM observations. This termination is then in equilibrium before the transformation proceeds via additional atom flips leading to another change in termination, whose mechanism is not easily found anymore. It should be noted that additional relaxation effects or the chemical order-disorder transition might play a role.

4.5.2 Observations on Al-Ni-Co$(001\bar{1}0)$

On the $(001\bar{1}0)$-surface the phase transition S1 ↔ basic Ni is observable by a characteristic step movement without any phase contrast. All steps split into two, one of them proceeding through the terrace to the next step as indicated by arrows in figure 4.27. There is no difference in work function observable in the MEM images indicating all planes to be of approximately the same composition. However, they must be structurally different to drive this surface phase transition. After the completion of one additional surface layer, an additional one is created by an equivalent movement of steps across the terraces.

4.5.3 S1 ↔ Basic Ni on the Tenfold (00001)-Surface

During the phase transition S1 ↔ basic Ni no remarkable observations can be made on the tenfold (00001)-surface. The material transport to or from the bulk, reflected in a step motion, is not observable on this surface, possibly because the steps of one atomic layer height are difficult to image due to their high mobility. Thus, the expected additional movement cannot be monitored. The structural transformations on the surface are not expected to change the morphology or

induce any phase contrast, since they are confined to the quasicrystalline planes. Hence, the absence of indications for this phase transition on the tenfold surface supports the interpretation of the data acquired on the twofold surfaces.

4.6 Surface Phase Transitions

One important characteristic of phase transitions is the order of the transformation between the respective modifications. In first order transitions, the involved phases are distinguishable from one another, implying the occurrence of a co-existence region. In contrast, higher order phase transformations are sharp, such that the respective phases are indistinguishable at the transition point and no co-existence region of multiple phases appears.

The surface phase transition around 730 °C clearly showed an equilibrium between the three different terminations. Anyhow, surface phase transitions are always expected show a phase co-existence, since long-range interactions on the surface, such as the elastic response to a difference in surface stress from differing surface phases, defects or steps and electrostatic fields, rule out any sharp transition [106]. Experimentally, Hannon et al. have supported this prediction by relating the phase coexistence on Si(111) during the phase transition (7 x 7) to (1 x 1) to elastic and electrostatic effects only, and claim this to be a universal feature of surface phase transitions [107].

In case of the phase transition at 650 °C, i.e., between the decagonal modifications type I and S1, the main observation was the material exchange with the bulk and a roughening/smoothing. However, the rough morphology was considered not to be in equilibrium, therefore not having completed the surface phase transition. Both bulk transformations are reported to be of second order as interpreted from dilatometric investigations [81, 108].

4.7 Conclusions and Outlook

In this chapter the morphology of the tenfold (00001)-, and the twofold (10000)- and (00$1\bar{1}$0)-surfaces of decagonal $Al_{72.3}Ni_{18.2}Co_{9.5}$ has been characterized in a temperature range from 30 ° to 850 °. At temperatures below 650 ° all surfaces are found to be very rough, while at higher temperature they exhibit flat terraces of μm size. On the twofold surfaces these are separated by stiff steps, while the steps on the tenfold surface are mobile due to their small height of a single layer spacing.

The smoothing/roughening has been found to coincide with a structural bulk phase transition (type I $\leftrightarrow$ S1), whose effect is visible by a strong material exchange between bulk and surface related to the creation/annihilation of structural bulk vacancies. Two mechanisms which support

the mass transport are observed: first, surface steps acting as sources or sinks for vacancies, and second, bulk channels, which assemble material via bulk diffusion and then bring it to the surface. The rough surface is probably not the equilibrium morphology of the type I phase due to insufficient diffusion below the transition point.

Although a quasiperiodic ordering perpendicular to the surface results in infinitely many inequivalent terminations, structurally similar net planes with high atom densities are responsible for the formation of the step-terrace morphology. These can easily be identified in the tiling-cluster models of the respective modifications.

On the twofold $(00\bar{1}0)$-surface the type I $\leftrightarrow$ S1 phase transition is accompanied by a faceting transition. The formation and dissipation of (10000)-equivalent facets has been described in detail. Their stability in the low temperature phase is explained by net planes of low surface free energy. The phase transition lowers the differences in surface free energy of (10000)- and $(00\bar{1}0)$-net-planes with respect to each other, thus inducing the facet dissipation at high temperatures.

Moreover, the S1 $\leftrightarrow$ basic Ni structural phase transition has been investigated on the surfaces. On the (10000)-surface a strong difference in work function of the S1 and basic Ni termination and an intermediate equilibrium state is observed. The basic Ni termination is thereby concluded to be more Al-rich than the lower temperature terminations.

For future studies it would be of particular interest to resolve the structure of the twofold surface terminations, as these could indicate a reason for their low surface free energy, and thus explain their stability. The measurement of stoichiometric surface composition and step heights might be sufficient to determine the energetically favored terminations by a comparison to structural models.

To a surface scientist, it is important to know how to prepare equilibrium surfaces. While the high temperature phases are very quickly equilibrated, cooling through the lowest phase transition leads to a non-equilibrium morphology. However, earlier experimental investigations show that the terraces of the room temperature surfaces exhibit a structure equivalent to a bulk termination [11, 13, 22, 75, 76]. Thus experiments, which do not rely on an equilibrated morphology can nonetheless yield new insights.